Journal of the Mechanics and Physics of Solids 57 (2009) 1828–1850

Contents lists available at ScienceDirect

Journal of the Mechanics and Physics of Solids

journal homepage: www.elsevier.com/locate/jmps

Onset of macroscopic instabilities in fiber-reinforced elastomers at finite strain

M. Agoras [a], O. Lopez-Pamies [b], P. Ponte Castañeda [a,*]

[a] Department of Mechanical Engineering and Applied Mechanics, University of Pennsylvania, Philadelphia, PA 19104-6315, USA
[b] Department of Mechanical Engineering, State University of New York, Stony Brook, NY 11794-2300, USA

ARTICLE INFO

Article history:
Received 3 February 2009
Received in revised form
29 July 2009
Accepted 3 August 2009

Keywords:
Fiber-reinforced composite
Finite strain
Microstructures
Instabilities
Homogenization

ABSTRACT

In this paper, we investigate theoretically the possible development of instabilities in fiber-reinforced elastomers (and other soft materials) when they are subjected to finite-strain loading conditions. We focus on the physically relevant class of "macroscopic" instabilities, i.e., instabilities with wavelengths that are much larger than the characteristic size of the underlying microstructure. To this end, we make use of recently developed homogenization estimates, together with a fundamental result of Geymonat, Müller and Triantafyllidis linking the development of these instabilities to the loss of strong ellipticity of the homogenized constitutive relations. For the important class of material systems with very stiff fibers and random microstructures, we derive a *closed-form* formula for the critical macroscopic deformation at which instabilities may develop under *general* loading conditions, and we show that this critical deformation is quite sensitive to the loading orientation relative to the fiber direction. The result is also confronted with classical estimates (including those of Rosen) for laminates, which have commonly been used as two-dimensional (2-D) approximations for actual fiber-reinforced composites. We find that while predictions based on laminate models are qualitatively correct for certain loadings, they can be significantly off for other more general 3-D loadings. Finally, we provide a parametric analysis of the effects of the matrix and fiber properties and of the fiber volume fraction on the onset of instabilities for various loading conditions.

1. Introduction

Many "soft" material systems of current interest exhibit an underlying fiber-reinforced structure. Prominent examples include a wide variety of soft biological tissues (see, e.g., Finlay et al., 1998; Quapp and Weiss, 1998) and nano-structured block copolymers (see, e.g., Honeker and Thomas, 1996; Honeker et al., 2000). From the theoretical point of view, several efforts within the past few years have been devoted to construct constitutive models that accurately describe the macroscopic mechanical behavior—i.e., the stress–strain relation—of such classes of reinforced materials subjected to *finite deformations* (see, e.g., Qiu and Pence, 1997; Holzapfel et al., 2000; Merodio and Ogden, 2005; deBotton, 2005; deBotton et al., 2006; Guo et al., 2006; Brun et al., 2007; Agoras et al., 2008). By contrast, the study of instabilities in these systems—although of great practical importance—has received comparatively little attention, presumably because of the intrinsic technical difficulties. In fact, most of the work to date seems to have been restricted primarily to studying the loss

* Corresponding author.
E-mail addresses: oscar.lopez-pamies@sunysb.edu (O. Lopez-Pamies), ponte@seas.upenn.edu (P. Ponte Castañeda).

0022-5096/$ - see front matter © 2009 Elsevier Ltd. All rights reserved.
doi:10.1016/j.jmps.2009.08.001

of ellipticity of phenomenological constitutive relations from a qualitative standpoint (see, e.g., Triantafyllidis and Abeyaratne, 1983; Merodio and Pence, 2001; Merodio and Ogden, 2003). It is appropriate to recall, however, that many researchers have utilized laminates as a two-dimensional (2-D) approximation of fiber-reinforced materials, starting with the pioneering work of Rosen (1965). Along these lines, a complete analysis of instabilities for hyperelastic laminates has been carried out by Triantafyllidis and co-workers by means of the Floquet theory for ODEs (see, e.g., Triantafyllidis and Maker, 1985; Nesterovic and Triantafyllidis, 2004). Another approximate approach to microbuckling in fiber-reinforced composites consists in modeling the fibers as beams on an elastic foundation (see, e.g., Grandidier and Poitier-Ferry, 1990).

The purpose of the present paper is to investigate the onset of "macroscopic" instabilities for a general class of fiber-reinforced *nonlinearly elastic* materials consisting of a soft matrix reinforced by a single family of stiff, aligned, cylindrical fibers that are distributed *randomly* and isotropically in the transverse plane, when subjected to arbitrary finite strains. To this end, we adopt a fundamental result of Geymonat et al. (1993) which states that the onset of long-wavelength instabilities—i.e., wavelengths that are much larger than the characteristic size of the underlying microstructure—in (a rather general class of) heterogeneous hyperelastic materials may be expediently computed from the loss of strong ellipticity of the corresponding homogenized properties. Furthermore, these so-called "macroscopic" instabilities provide a rigorous upper bound for other types of instabilities with finite wavelengths, called "microscopic" instabilities. In this connection, we should mention the work of Abdelmoula et al. (1993) which attempted a first study of microscopic and macroscopic instabilities in fiber-reinforced elastomers; however, the final results provided were also for a 2-D laminate model.

The approach discussed in the previous paragraph to determine the onset of macroscopic instabilities requires the knowledge of the homogenized behaviors of the materials of interest. But the problem of computing the homogenized properties of fiber-reinforced nonlinearly elastic materials, subjected to finite deformations—especially with random microstructures—is quite a difficult task in itself. Indeed, *exact* homogenization results are only accessible for particular loading conditions, special microstructures, and restricted local (matrix and fiber) constitutive behaviors (He et al., 2006). *Approximate* results have also remained elusive until very recently. In addition to the elementary Voigt (Ogden, 1978) and polyconvex (Ponte Castañeda, 1989) bounds, there is the estimate of deBotton et al. (2006) (see also Guo et al., 2006) for fiber-reinforced materials with incompressible Neo-Hookean matrix and fiber phases, and certain special types of microstructures.

In this work, we will make use of the "variational linear comparison" estimate recently developed by Agoras et al. (2008) to model the homogenized properties of a large class of fiber-reinforced nonlinearly elastic materials. Specifically, the proposed estimate applies to materials with *random* transversely isotropic distribution of fibers and with matrix and fiber constituents that are characterized by a *general class* of incompressible, isotropic stored-energy functions. (A corresponding estimate for material systems with *compressible* generalized Neo-Hookean constituents and *periodic* microstructures has been given by Brun et al., 2007.) The estimate of Agoras et al. (2008) was derived by making combined use of the works of Ponte Castañeda and Tiberio (2000) and Lopez-Pamies and Ponte Castañeda (2006a), which in turn provide generalizations of the "second-order" methods of Ponte Castañeda (1996, 2002), respectively, for hyperelastic composites. Besides its generality, the estimate of Agoras et al. (2008) has the merit that it recovers known exact results for special loading conditions. Moreover, it accounts for fine statistical information about the *initial* microstructure beyond the volume fraction of fibers, as well as for its *evolution*, which results from the finite changes in geometry that are induced by the applied finite deformations. This feature is of the essence in the present context, as the evolution of microstructure can have a significant *geometric* softening (or stiffening) effect on the macroscopic response of the material, which may ultimately lead to the development of instabilities (see, e.g., the work of Lopez-Pamies and Ponte Castañeda, 2009). In addition to the estimate of Agoras et al. (2008), we will also consider the estimate of deBotton et al. (2006)—which, as already stated, applies to the restricted but important case of materials with Neo-Hookean matrix and fiber constituents—to approximate the homogenized response of fiber-reinforced nonlinearly elastic materials.

The structure of the paper is as follows. First, in Section 2 we describe in detail the (microgeometries and local constitutive behaviors of the) class of fiber-reinforced materials under study in this work. In addition, this section spells out the homogenized response of these materials under arbitrary finite deformations, as characterized by the estimates of Agoras et al. (2008) and of deBotton et al. (2006). In Section 3, the condition of strong ellipticity—used to determine the "macroscopic" instabilities—is recalled in general and then specialized to the constitutive relations of Agoras et al. (2008) and deBotton et al. (2006). Making use of the relations put forward in Sections 2 and 3, results for the onset of instabilities in fiber-reinforced elastic materials subjected to finite deformations are then derived in Sections 4 and 5 for aligned and non-aligned loading conditions, respectively. In Section 6, we derive a closed-form formula (see also Eq. (1)) for the possible development of instabilities under *general* loading conditions in Neo-Hookean composites, and show that the result also applies, approximately, for more general material behavior, provided that the fiber–matrix heterogeneity contrast is sufficiently large. In Sections 4–6, we also make comparisons with classical results from the literature, as well as with new results, for 2-D laminate models. These comparisons serve to elucidate the limitations of the use of the 2-D laminate approximation for general loading conditions. Finally, some concluding remarks will be drawn in Section 7.

The main result of this paper can be summarized as follows: *along an arbitrary loading path with average deformation gradient* $\overline{\mathbf{F}}$, *macroscopic instabilities may develop in fiber-reinforced nonlinearly elastic materials whenever the stretch in the fiber*

direction reaches the critical value

$$\overline{\lambda}_n = \|\overline{\mathbf{F}}\mathbf{N}\| = \left(1 - \frac{\widetilde{\mu}_n}{\widetilde{\mu}_a}\right)^{1/3}. \tag{1}$$

Here, the unit vector $\mathbf{N}$ characterizes the direction of the fibers in the undeformed configuration, while $\widetilde{\mu}_n$ and $\widetilde{\mu}_a$ denote, respectively, the effective longitudinal and axisymmetric shear moduli of the fiber-reinforced composite in the ground state.

2. Homogenization estimates for fiber-reinforced hyperelastic materials

The composites considered in this work consist of a matrix material (phase 1) reinforced by a single family of aligned, cylindrical fibers (phase 2) with initially circular cross-section. For definiteness, the initial direction of fiber alignment is denoted by the unit vector $\mathbf{N}$ (see Fig. 1(a)). The distribution of fibers in the transverse plane (i.e., perpendicular to $\mathbf{N}$) is taken to be random and isotropic in the undeformed configuration Ω_0. It is further assumed that the average diameter of the fibers is much smaller than the size of a typical macroscopic specimen; in other words, the macroscopic and microscopic length scales are well separated. Moreover, the constitutive behaviors of the phases are taken to be characterized by the general class of incompressible, isotropic stored-energy functions of the form

$$W^{(r)}(\mathbf{F}) = g^{(r)}(I) \quad (r = 1, 2) \tag{2}$$

subject to the incompressibility constraint $\det\mathbf{F} = 1$ (i.e., $W^{(r)}(\mathbf{F}) = +\infty$ if $\det\mathbf{F} \neq 1$). Here, $\mathbf{F}$ denotes the deformation gradient tensor, $I = I_1 = \operatorname{tr}\mathbf{C}$ stands for the first principal invariant of the right Cauchy–Green deformation tensor $\mathbf{C} = \mathbf{F}^T\mathbf{F}$, and $g^{(r)}$ can be any differentiable material function satisfying the linearization conditions: $g^{(r)}(3) = 0$ and $g_I^{(r)}(3) = \mu^{(r)}/2$, where $\mu^{(r)}$ denotes the small-strain shear modulus of phase r, and the notation $g_I^{(r)}(\cdot) = dg^{(r)}(\cdot)/dI$ has been introduced for convenience.

A simple example of a stored-energy function of the form (2), which does capture the limiting chain extensibility of rubber-like solids, is the Gent (1996) material

$$W(\mathbf{F}) = g(I) = -\frac{J_m\mu}{2}\ln\left[1 - \frac{I-3}{J_m}\right]. \tag{3}$$

In this relation, the parameter J_m corresponds to the maximum deformation, as measured by $I-3$, that the material may undergo before it locks up. Note that, in the limit as $J_m \to \infty$, expression (3) reduces identically to the Neo-Hookean model

$$W(\mathbf{F}) = g(I) = \frac{\mu}{2}(I-3). \tag{4}$$

The functional form of the homogenized (or macroscopic) response of the above-described fiber-reinforced nonlinearly elastic materials can be shown (Hill, 1972) to be characterized by an *effective* hyperelastic potential, $\widehat{W}$, that is a transversely isotropic scalar function (with symmetry axis $\mathbf{N}$) of the macroscopic deformation gradient tensor $\overline{\mathbf{F}}$, subject to the macroscopic incompressibility constraint $\det\overline{\mathbf{F}} = 1$ (i.e., $\widehat{W}(\overline{\mathbf{F}}) = +\infty$ if $\det\overline{\mathbf{F}} \neq 1$). More specifically, $\widehat{W}$ depends on $\overline{\mathbf{F}}$ and $\mathbf{N}$ only through the four (canonical) transversely isotropic invariants: $\overline{I}_1 = \operatorname{tr}\overline{\mathbf{C}}$, $\overline{I}_2 = (1/2)((\operatorname{tr}\overline{\mathbf{C}})^2 - \operatorname{tr}\overline{\mathbf{C}}^2)$, $\overline{I}_4 = \mathbf{N}\cdot\overline{\mathbf{C}}\mathbf{N}$, $\overline{I}_5 = \mathbf{N}\cdot\overline{\mathbf{C}}^2\mathbf{N}$. In this work, we will make use of the equivalent set of invariants (see Ericksen and Rivlin, 1954; deBotton et al., 2006):

$$\begin{aligned}&\overline{\lambda}_n = [(\overline{\mathbf{F}}\mathbf{N})\cdot(\overline{\mathbf{F}}\mathbf{N})]^{1/2}, \quad \overline{\gamma}_n = [(\overline{\mathbf{F}}^T\overline{\mathbf{F}}\mathbf{N})\cdot(\overline{\mathbf{F}}^T\overline{\mathbf{F}}\mathbf{N}) - \overline{\lambda}_n^4]^{1/2}/\overline{\lambda}_n,\\ &\overline{\gamma}_p = (\overline{\mathbf{F}}\cdot\overline{\mathbf{F}} - \overline{\lambda}_n^2 - 2/\overline{\lambda}_n - \overline{\gamma}_n^2)^{1/2},\end{aligned} \tag{5}$$

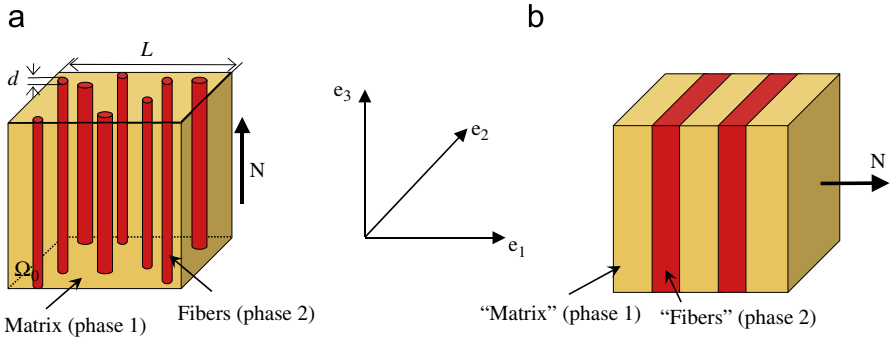

Fig. 1. (a) Schematic of a fiber-reinforced composite in the undeformed configuration Ω_0, where the initial fiber direction is given by the unit vector $\mathbf{N}$. (b) Corresponding schematic of a laminate with lamination direction $\mathbf{N}$. The characteristic lengths of the macroscopic specimen, L, and of the fibers (or layers), d, are assumed to be well separated in the sense that $L \gg d$.

and $\overline{\psi}_\gamma$ (which depends on $\overline{I}_2$). These invariants, which can be easily written in terms of the first set, have the advantage of a more direct physical interpretation: $\overline{\lambda}_n$ denotes the stretch along the fiber direction $\mathbf{N}$, $\overline{\gamma}_n$ corresponds to the longitudinal (antiplane) shear, and $\overline{\gamma}_p$ stands for the shear in the transverse plane (in-plane shear).

The precise determination of $\widehat{W}$, however, is a difficult problem and, as a result, exact solutions are accessible only for very particular loading conditions and special local (matrix and fiber) constitutive behaviors (see, e.g., He et al., 2006). In the sequel, in order to approximate the homogenized behavior of the above-described general class of materials under arbitrary loading conditions, we will make use of the *variational linear comparison* estimate proposed recently by Agoras et al. (2008). We will also make use of the earlier estimate of deBotton et al. (2006), which applies only to the special case of Neo-Hookean behavior for the matrix and fiber phases.

2.1. The estimate of Agoras et al. for generalized Neo-Hookean phases

By making use of the variational procedures of Lopez-Pamies and Ponte Castañeda (2006a) and Ponte Castañeda and Tiberio (2000), Agoras et al. (2008) have constructed an estimate for the effective stored-energy function $\widehat{W}$ of the fiber-reinforced materials described above, which was found to be rather insensitive to $\overline{\psi}_\gamma$, so that $\widehat{W}(\overline{\mathbf{F}}) = \widehat{\Phi}(\overline{\lambda}_n, \overline{\gamma}_p, \overline{\gamma}_n)$. The specific expression for $\widehat{\Phi}$ is given by

$$\widehat{\Phi}(\overline{\lambda}_n, \overline{\gamma}_p, \overline{\gamma}_n) = (1-c_0)[g^{(1)}(\hat{I}^{(1)}) + g_{\mathrm{I}}^{(1)}(I^{(1)})\overline{\gamma}_n^{(1)}(\overline{\gamma}_n - \overline{\gamma}_n^{(1)})] + c_0[g^{(2)}(I^{(2)}) + g_{\mathrm{I}}^{(2)}(I^{(2)})\overline{\gamma}_n^{(2)}(\overline{\gamma}_n - \overline{\gamma}_n^{(2)})], \tag{6}$$

where c_0 denotes the initial volume fraction of fibers, it is recalled that $g_I^{(r)} = dg^{(r)}/dI$, and

$$\begin{aligned}
\hat{I}^{(1)} &= \left(\frac{\overline{\lambda}_1 - c_0\overline{\lambda}_1^{(2)}}{1-c_0}\right)^2 + \left(\frac{\overline{\lambda}_2 - c_0\overline{\lambda}_2^{(2)}}{1-c_0}\right)^2 + \overline{\lambda}_n^2 + (\overline{\gamma}_n^{(1)})^2 + c_0\left(\frac{\overline{\lambda}_1 - \overline{\lambda}_1^{(2)}}{(1-c_0)\overline{\lambda}_1^{(2)}\overline{\lambda}_1\overline{\lambda}_n}\right)^2[(\overline{\lambda}_1^{(2)}\overline{\lambda}_1\overline{\lambda}_n + 1)^2 + (\overline{\lambda}_1^2 + (\overline{\lambda}_1^{(2)})^2)\overline{\lambda}_n],\\
I^{(1)} &= \overline{\lambda}_1^2 + \overline{\lambda}_2^2 + \overline{\lambda}_n^2 + (\overline{\gamma}_n^{(1)})^2,\\
I^{(2)} &= (\overline{\lambda}_1^{(2)})^2 + (\overline{\lambda}_2^{(2)})^2 + \overline{\lambda}_n^2 + (\overline{\gamma}_n^{(2)})^2.
\end{aligned} \tag{7}$$

In these expressions,

$$\begin{aligned}
\overline{\lambda}_1 &= \frac{\sqrt{\overline{\gamma}_p^2 + 4/\overline{\lambda}_n} - \overline{\gamma}_p}{2}, \quad \overline{\lambda}_2 = \frac{\sqrt{\overline{\gamma}_p^2 + 4/\overline{\lambda}_n} + \overline{\gamma}_p}{2},\\
\overline{\lambda}_2^{(2)} &= \frac{1}{\overline{\lambda}_1^{(2)}\overline{\lambda}_n}, \quad \overline{\gamma}_n^{(2)} = \frac{\overline{\gamma}_n - (1-c_0)\overline{\gamma}_n^{(1)}}{c_0},
\end{aligned} \tag{8}$$

and the variables $\overline{\lambda}_1^{(2)}$ and $\overline{\gamma}_n^{(1)}$ are the solution of the following system of two coupled, nonlinear, algebraic equations:

$$\mathscr{E}_1(\overline{\lambda}_1^{(2)}, \overline{\gamma}_n^{(1)}) = \sqrt{g_{\mathrm{I}}^{(1)}(I^{(1)})[g_{\mathrm{I}}^{(1)}(I^{(1)}) + 2g_{\mathrm{II}}^{(1)}(I^{(1)})(\overline{\gamma}_n^{(1)})^2]}(\overline{\gamma}_n - \overline{\gamma}_n^{(1)}) + c_0(g_{\mathrm{I}}^{(2)}(I^{(2)})\overline{\gamma}_n^{(2)} - g_{\mathrm{I}}^{(1)}(I^{(1)})\overline{\gamma}_n^{(1)}) = 0, \tag{9}$$

$$\begin{aligned}
\mathscr{E}_2(\overline{\lambda}_1^{(2)}, \overline{\gamma}_n^{(1)}) &= [(1+c_0)g_{\mathrm{I}}^{(1)}(\hat{I}^{(1)}) + (1-c_0)g_{\mathrm{I}}^{(2)}(I^{(2)})](\overline{\lambda}_n^{-2} - (\overline{\lambda}_1^{(2)})^4) - g_{\mathrm{I}}^{(1)}(\hat{I}^{(1)})\left[2\overline{\lambda}_1^{(2)}\overline{\lambda}_1(\overline{\lambda}_2^2 - (\overline{\lambda}_1^{(2)})^2) - \frac{(\overline{\lambda}_1^4 - (\overline{\lambda}_1^{(2)})^4)\overline{\lambda}_2}{\overline{\lambda}_1}\right]\\
&= 0,
\end{aligned} \tag{10}$$

where the notation $g_{\mathrm{II}}^{(1)}(\cdot) = d^2g^{(1)}(\cdot)/dI^2$ has been employed in (9) for convenience. For a detailed description of the derivation and of the various quantities involved in the above estimate, we refer to Agoras et al. (2008). In the present context, it is appropriate to remark that the result (6) incorporates one-point (the volume fraction of fibers) and two-point (the cylindrical shape and random and transversely isotropic distribution of fibers) statistical information about the underlying *initial* microstructure. Furthermore, it also accounts for the *evolution* of such a microstructure, which results from the applied finite deformations. This feature is of critical importance since the evolution of microstructure can have significant softening (or stiffening) effect that may ultimately lead to the development of instabilities. In addition, the estimate (6) has the merit that it recovers known exact results for special loading conditions, including the case of aligned axisymmetric shear (He et al., 2006). Moreover, full numerical simulations (Moraleda et al., 2009) have also established that the estimate (6) leads to remarkably accurate predictions for in-plane loading conditions (i.e., $\overline{\lambda}_n = 1$, $\overline{\gamma}_n = 0$), at least for Neo-Hookean phases. Finally, it is relevant to remark that the stored-energy function (6) linearizes properly, as it reduces to the corresponding estimate of Walpole (1969) in the limit as $\overline{\mathbf{F}} \to \mathbf{I}$, namely

$$\widehat{\Phi}(\overline{\lambda}_n, \overline{\gamma}_p, \overline{\gamma}_n) = \frac{\tilde{\mu}_a}{2}\overline{\varepsilon}_a^2 + \frac{\tilde{\mu}_p}{2}\overline{\varepsilon}_p^2 + \frac{\tilde{\mu}_n}{2}\overline{\varepsilon}_n^2 + O(\|\overline{\mathbf{F}} - \mathbf{I}\|^3). \tag{11}$$

Here, $\overline{\varepsilon}_a$, $\overline{\varepsilon}_p$, and $\overline{\varepsilon}_n$ are the axisymmetric, transverse, and longitudinal shear invariants of the infinitesimal strain tensor $\overline{\boldsymbol{\varepsilon}} = (1/2)(\overline{\mathbf{F}}^T + \overline{\mathbf{F}} - 2\mathbf{I})$ (see, e.g., deBotton and Ponte Castañeda, 1993), and $\tilde{\mu}_a$, $\tilde{\mu}_p$, and $\tilde{\mu}_p$ are the corresponding effective shear moduli in these three modes, which are given in terms of the shear moduli of the matrix and fibers, $\mu^{(1)}$ and $\mu^{(2)}$, and

the volume fraction of fibers, c_0, by

$$\widetilde{\mu}_a = (1-c_0)\mu^{(1)} + c_0\mu^{(2)} \equiv \overline{\mu} \tag{12}$$

and

$$\widetilde{\mu}_p = \widetilde{\mu}_n = \frac{(1-c_0)\mu^{(1)} + (1+c_0)\mu^{(2)}}{(1+c_0)\mu^{(1)} + (1-c_0)\mu^{(2)}}\mu^{(1)} \equiv \widetilde{\mu}. \tag{13}$$

Note that $\widetilde{\mu} \leq \overline{\mu}$, in general, and that $\widetilde{\mu} \ll \overline{\mu}$ in the limit of large heterogeneity contrast $t = \mu^{(2)}/\mu^{(1)} \gg 1$, which has the physical interpretation that the axisymmetric shear mode is controlled by the stiffer fibers, while the transverse and longitudinal shear modes are controlled by the softer matrix behavior.

2.2. The estimate of Agoras et al. for Neo-Hookean phases

For later reference, we spell out next the specialization of the general estimate (6) to materials with Neo-Hookean behavior (4) for the matrix and fiber constituents. To this end, first it is helpful to recognize that Eqs. (9) and (10) decouple into two independent equations for $\overline{\gamma}_n^{(1)}$ and $\overline{\lambda}_1^{(2)}$, respectively. The resulting equation (9) for $\overline{\gamma}_n^{(1)}$ can be solved in closed form rendering $\overline{\gamma}_n^{(1)} = (\mu^{(1)} + \mu^{(2)})\overline{\gamma}_n/((1+c_0)\mu^{(1)} + (1-c_0)\mu^{(2)})$, while (10) reduces to a nonlinear equation for $\overline{\lambda}_1^{(2)}$ shown below. After some algebraic manipulation, it is then straightforward to deduce that the stored-energy function (6) reduces to

$$\widehat{\Phi}(\overline{\lambda}_n, \overline{\gamma}_p, \overline{\gamma}_n) = (1-c_0)\frac{\mu^{(1)}}{2}(\hat{I}_P^{(1)} - 3) + c_0\frac{\mu^{(2)}}{2}(I_P^{(2)} - 3) + \frac{\widetilde{\mu}}{2}\overline{\gamma}_n^2, \tag{14}$$

where $\widetilde{\mu}$ is given by (13) and $\hat{I}_P^{(1)} = \hat{I}^{(1)} - (\overline{\gamma}_n^{(1)})^2$, $I_P^{(2)} = I^{(2)} - (\overline{\gamma}_n^{(2)})^2$ are ultimately functions of the unknown $\overline{\lambda}_1^{(2)}$, which is solution to the fourth-order polynomial equation

$$\mathscr{E}(\overline{\lambda}_1^{(2)}) = [(1+c_0)\mu^{(1)} + (1-c_0)\mu^{(2)}](\overline{\lambda}_n^{-2} - (\overline{\lambda}_1^{(2)})^4) - \mu^{(1)}\left[2\overline{\lambda}_1^{(2)}\overline{\lambda}_1(\overline{\lambda}_2^2 - (\overline{\lambda}_1^{(2)})^2) - \frac{(\overline{\lambda}_1^4 - (\overline{\lambda}_1^{(2)})^4)\overline{\lambda}_2}{\overline{\lambda}_1}\right] = 0. \tag{15}$$

2.3. The estimate of deBotton et al. for Neo-Hookean phases

As already mentioned, the effective stored-energy function (6) is the only available homogenization estimate for nonlinearly elastic fiber-reinforced composites allowing consideration of general constitutive behaviors (2) for the underlying matrix and fiber phases. However, in the simpler context of Neo-Hookean constituents with stored-energy functions of the form (4), deBotton et al. (2006) have derived the following estimate:

$$\widehat{\Phi}(\overline{\lambda}_n, \overline{\gamma}_p, \overline{\gamma}_n) = \frac{\overline{\mu}}{2}\left(\overline{\lambda}_n^2 + \frac{2}{\overline{\lambda}_n} - 3\right) + \frac{\widetilde{\mu}}{2}(\overline{\gamma}_p^2 + \overline{\gamma}_n^2), \tag{16}$$

where $\overline{\mu}$ and $\widetilde{\mu}$ have been defined by (12) and (13), respectively. It is worth remarking that $\overline{\gamma}_p$ and $\overline{\gamma}_n$ enter the above expression only as the sum $\overline{\gamma}_p^2 + \overline{\gamma}_n^2$, so that the model of deBotton et al. (16) actually depends *not* on 3 but only on 2 ($\bar{I}_1$ and $\bar{I}_4$) out of 4 ($\bar{I}_1, \bar{I}_2, \bar{I}_4, \bar{I}_5$) possible transversely isotropic invariants.

In spite of their different appearance, expressions (14) and (16) generally lead to similar overall stress–strain predictions. In particular, the stored-energy function (16) also linearizes according to relation (11). Moreover, expressions (14) and (16) can be shown to be identical for the case of antiplane combined with axisymmetric shear deformations (i.e., $\overline{\gamma}_p = 0$), which, incidentally, corresponds to an *exact* result for materials with the special "composite cylinder assemblage" microstructure of Hashin and Rosen (deBotton et al., 2006). The main difference between (14) and (16) appears for large values of the in-plane shear $\overline{\gamma}_p$ when—in agreement with full field simulations (Moraleda et al., 2009)—(14) leads to a noticeably stiffer response.

3. Onset of macroscopic instabilities

In a remarkable contribution, Geymonat et al. (1993) demonstrated rigorously that (i) the onset of "macroscopic" instabilities (or instabilities with wavelengths that are much larger than the characteristic size of the underlying microstructure) for a general class of heterogeneous hyperelastic materials can be determined from the *loss of strong ellipticity of the homogenized response*, and (ii) the onset of such long-wavelength instabilities constitutes a rigorous upper bound to the onset of any other type of instabilities with finite wavelength (i.e., "microscopic" instabilities). From a practical point of view, the importance of these theoretical results derives from the fact that the "macroscopic" instabilities are much easier to compute (assuming that the homogenized response is available) than the "microscopic" ones. In fact, there is no feasible procedure for computing "microscopic" instabilities for composites with random microstructures, such as the ones of interest in this work. Moreover, it is often the case that first instabilities are of the long-wavelength type. For example, for the laminated materials considered by Triantafyllidis and Maker (1985) and by Nesterovic and Triantafyllidis (2004) under plane-strain loading conditions, the first instabilities are always of long wavelength, at least for sufficiently

large concentrations of the reinforcing phase. Furthermore, recent work by Michel et al. (2009) in the context of particulate reinforced elastomers has demonstrated that at least the microscopic instabilities that are related to the periodicity of the microstructure tend to disappear as the microstructure is perturbed (randomly) away from a purely periodic state, which suggests that the "macroscopic" instabilities may in some sense be the most relevant ones for random composites anyway.

For the type of fiber-reinforced materials of interest here, the first instabilities to be encountered along arbitrary loading paths are expected to be of the long-wavelength type, at least for fiber concentrations that are not too small. Thus, for materials with *sufficiently large* volume fraction of fibers, the loss of strong ellipticity of the homogenized behavior, at appropriate critical strains, would be expected to indicate accurately the development of first instabilities. For materials with very *small* volume fractions of fibers, on the other hand, the loss of strong ellipticity of the homogenized response may *not* signal the onset of the first instabilities (something else may happen), but this condition is expected to provide, however, a useful upper bound for them.

We recall next the condition of strong ellipticity and spell out its specialization to the *estimates* (6), (14), and (16) for the homogenized behavior of fiber-reinforced nonlinearly elastic materials; these conditions will then be used in the next sections to estimate the onset of macroscopic instabilities in these materials under arbitrary loading conditions. Quite generally, strong ellipticity of a given constitutive relation corresponds to positive definiteness of the associated acoustic tensor. In particular, for a hyperelastic constitutive relation characterized by an *incompressible* stored-energy function $\widehat{W}(\overline{\mathbf{F}})$—such as the one of interest in this work—the condition of strong ellipticity may be written as

$$\widehat{\mathscr{L}}^{c}_{ijkl}(\overline{\mathbf{F}})v_j v_l u_i u_k > 0 \tag{17}$$

for all unit vectors $\mathbf{v}$ and $\mathbf{u}$ that satisfy the *incompressibility constraint* $\mathbf{v}\cdot\mathbf{u}=0$. In the above expression, $\widehat{\mathscr{L}}^{c}_{ijkl}(\overline{\mathbf{F}}) = \overline{F}_{jp}\overline{F}_{lq}\partial^2\widehat{W}(\overline{\mathbf{F}})/\partial\overline{F}_{ip}\partial\overline{F}_{kq}$ stands for the incremental tangent modulus in the current (deformed) configuration, hence the superscript c (see, e.g., Chapter 6.2.7 in the monograph by Ogden, 1984).

As already noted above, the stored-energy function $\widehat{W}$ for the fiber-reinforced materials of interest in this work should linearize according to relation (11). Given that $\tilde{\mu}_a$, $\tilde{\mu}_p$, and $\tilde{\mu}_n$, as defined by expressions (12) and (13) are all positive, it follows that $\widehat{W}$ is strictly convex in the infinitesimal strain $\overline{\boldsymbol{\varepsilon}}$ for sufficiently small deformations. As a result, condition (17) is expected to hold true in some small neighborhood of $\overline{\mathbf{F}}=\mathbf{I}$, except possibly in the case of rigid fibers, when condition (17) may be violated at exactly $\overline{\mathbf{F}}=\mathbf{I}$. Along arbitrary loading paths, however, as the deformation progresses beyond $\overline{\mathbf{F}}=\mathbf{I}$ into the finite-deformation regime, a point may be reached at which condition (17) ceases to hold true for some critical $\overline{\mathbf{F}}_{cr}$ and pair of critical vectors $\mathbf{v}_{cr}$ and $\mathbf{u}_{cr}$. The set of all such critical values $\overline{\mathbf{F}}_{cr}$ defines a hypersurface in deformation space delimiting strongly elliptic from non-strongly elliptic regions for the material response. In addition, the associated critical pairs of orthogonal vectors $\mathbf{v}_{cr}$ and $\mathbf{u}_{cr}$ describe the manner in which the material loses strong ellipticity. In particular, $\mathbf{v}_{cr}$ denotes the normal (in the deformed configuration) to a band (or bands) within which the material softens drastically and the deformation is thus prone to localize. On the other hand, the vector $\mathbf{u}_{cr}$ denotes the direction (also in the deformed configuration) along which the material softens within the band (or bands).

The estimate of Agoras et al.: The general condition (17) simplifies considerably when specialized to a stored-energy function $\widehat{W}$ depending on $\overline{\mathbf{F}}$ (and $\mathbf{N}$) only through the invariants $\overline{\lambda}_n$, $\overline{\gamma}_p$ and $\overline{\gamma}_n$, which is the case for all estimates considered in this work. Indeed, using (5) to express $\overline{\lambda}_n$, $\overline{\gamma}_p$ and $\overline{\gamma}_n$ as functions of $\overline{\mathbf{F}}$ and $\mathbf{N}$, together with the chain rule, the condition of strong ellipticity for a stored-energy function of the form $\widehat{W}(\overline{\mathbf{F}}) = \widehat{\Phi}(\overline{\lambda}_n, \overline{\gamma}_p, \overline{\gamma}_n)$ can be shown to reduce to

$$\sum_{i=1}^{3}(\alpha_i E_i + \beta_{ii}G_{ii}) + \beta_{12}G_{12} + \beta_{13}G_{13} + \beta_{23}G_{23} > 0. \tag{18}$$

In this relation,

$$\begin{aligned}
&E_1 = \mathbf{v}\cdot\overline{\mathbf{B}}\mathbf{v}, \quad E_2 = \overline{\lambda}_n^2(\mathbf{n}\cdot\mathbf{v})^2,\\
&E_3 = \overline{\lambda}_n^2[((\mathbf{n}\cdot\mathbf{v})\mathbf{u}+(\mathbf{n}\cdot\mathbf{u})\mathbf{v})\cdot\overline{\mathbf{B}}((\mathbf{n}\cdot\mathbf{v})\mathbf{u}+(\mathbf{n}\cdot\mathbf{u})\mathbf{v}) + 2(\mathbf{n}\cdot\mathbf{v})(\mathbf{n}\cdot\overline{\mathbf{B}}\mathbf{v})],\\
&G_{11} = (\mathbf{v}\cdot\overline{\mathbf{B}}\mathbf{u})^2, \quad G_{22} = \overline{\lambda}_n^4(\mathbf{n}\cdot\mathbf{v})^2(\mathbf{n}\cdot\mathbf{u})^2,\\
&G_{33} = \overline{\lambda}_n^4[(\mathbf{n}\cdot\mathbf{v})(\mathbf{n}\cdot\overline{\mathbf{B}}\mathbf{u}) + (\mathbf{n}\cdot\mathbf{u})(\mathbf{n}\cdot\overline{\mathbf{B}}\mathbf{v})]^2,\\
&G_{12} = 2\overline{\lambda}_n^2(\mathbf{n}\cdot\mathbf{v})(\mathbf{n}\cdot\mathbf{u})(\mathbf{v}\cdot\overline{\mathbf{B}}\mathbf{u}),\\
&G_{13} = 2\overline{\lambda}_n^2(\mathbf{v}\cdot\overline{\mathbf{B}}\mathbf{u})[(\mathbf{n}\cdot\mathbf{v})(\mathbf{n}\cdot\overline{\mathbf{B}}\mathbf{u}) + (\mathbf{n}\cdot\mathbf{u})(\mathbf{n}\cdot\overline{\mathbf{B}}\mathbf{v})],\\
&G_{23} = 2\overline{\lambda}_n^4(\mathbf{n}\cdot\mathbf{v})(\mathbf{n}\cdot\mathbf{u})[(\mathbf{n}\cdot\mathbf{v})(\mathbf{n}\cdot\overline{\mathbf{B}}\mathbf{u}) + (\mathbf{n}\cdot\mathbf{u})(\mathbf{n}\cdot\overline{\mathbf{B}}\mathbf{v})],
\end{aligned} \tag{19}$$

where $\overline{\mathbf{B}} = \overline{\mathbf{F}}\,\overline{\mathbf{F}}^T$ is the left Cauchy–Green deformation tensor and $\mathbf{n} = \overline{\lambda}_n^{-1}\overline{\mathbf{F}}\mathbf{N}$ denotes the direction of the fibers in the deformed configuration. The rest of the quantities in expression (18) depend inherently on the derivatives of $\widehat{\Phi}$ with respect

to its arguments $\overline{\lambda}_n$, $\overline{\gamma}_p$, $\overline{\gamma}_n$, and they are given by

$$\alpha_1=\frac{1}{\overline{\gamma}_p}\frac{\partial\widehat{\Phi}}{\partial\overline{\gamma}_p},\quad \alpha_3=\frac{1}{\overline{\lambda}_n^2}\left(\frac{1}{\overline{\gamma}_n}\frac{\partial\widehat{\Phi}}{\partial\overline{\gamma}_n}-\frac{1}{\overline{\gamma}_p}\frac{\partial\widehat{\Phi}}{\partial\overline{\gamma}_p}\right),$$
$$\alpha_2=\frac{1}{\overline{\lambda}_n}\frac{\partial\widehat{\Phi}}{\partial\overline{\lambda}_n}+\frac{1}{\overline{\gamma}_p}\frac{\partial\widehat{\Phi}}{\partial\overline{\gamma}_p}\left(\frac{\overline{\gamma}_n^2}{\overline{\lambda}_n^2}+\frac{1}{\overline{\lambda}_n^3}+1\right)-\frac{1}{\overline{\gamma}_n}\frac{\partial\widehat{\Phi}}{\partial\overline{\gamma}_n}\left(\frac{\overline{\gamma}_n^2}{\overline{\lambda}_n^2}+2\right),$$
$$\beta_{1i}=\frac{1}{\overline{\gamma}_p}\frac{\partial\alpha_i}{\partial\overline{\gamma}_p},\quad \beta_{3i}=\frac{1}{\overline{\lambda}_n^2}\left(\frac{1}{\overline{\gamma}_n}\frac{\partial\alpha_i}{\partial\overline{\gamma}_n}-\frac{1}{\overline{\gamma}_p}\frac{\partial\alpha_i}{\partial\overline{\gamma}_p}\right),$$
$$\beta_{2i}=\frac{1}{\overline{\lambda}_n}\frac{\partial\alpha_i}{\partial\overline{\lambda}_n}+\frac{1}{\overline{\gamma}_p}\frac{\partial\alpha_i}{\partial\overline{\gamma}_p}\left(\frac{\overline{\gamma}_n^2}{\overline{\lambda}_n^2}+\frac{1}{\overline{\lambda}_n^3}+1\right)-\frac{1}{\overline{\gamma}_n}\frac{\partial\alpha_i}{\partial\overline{\gamma}_n}\left(\frac{\overline{\gamma}_n^2}{\overline{\lambda}_n^2}+2\right)\tag{20}$$

with $i=1,2,3$. Note that the above choice for the variables β_{ij} leads to the symmetry $\beta_{ij}=\beta_{ji}$.

For the special case of the estimate (6) of Agoras et al. (2008) the explicit expressions for $\partial\widehat{\Phi}/\partial\overline{\lambda}_n$, $\partial\widehat{\Phi}/\partial\overline{\gamma}_p$, $\partial\widehat{\Phi}/\partial\overline{\gamma}_n$ and higher order derivatives of $\widehat{\Phi}$ in (20) are too cumbersome to be included here. For our purposes, in any case, it suffices to point out that they are known *closed-form* functions of the macroscopic loading parameters $\overline{\lambda}_n$, $\overline{\gamma}_p$, $\overline{\gamma}_n$, as well as of $\overline{\lambda}_1^{(2)}$, $\overline{\gamma}_n^{(1)}$, which are the solution of the system of Eqs. (9) and (10).

The estimate of Agoras et al. for Neo-Hookean phases: The general strong ellipticity condition (18), together with (19) and (20), when specialized to estimate (14) for Neo-Hookean phases, simplifies to

$$\begin{aligned}&\frac{1}{\overline{\gamma}_p^2}\left(\frac{\partial^2\widehat{\Phi}}{\partial\overline{\gamma}_p^2}-\frac{1}{\overline{\gamma}_p}\frac{\partial\widehat{\Phi}}{\partial\overline{\gamma}_p}\right)\left[G_{11}-\frac{G_{13}}{\overline{\lambda}_n^2}+\frac{G_{33}}{\overline{\lambda}_n^4}+\left(\frac{\overline{\gamma}_n^2}{\overline{\lambda}_n^2}+\frac{1}{\overline{\lambda}_n^3}+1\right)\left(G_{12}-\frac{G_{23}}{\overline{\lambda}_n^2}+G_{22}\left(\frac{\overline{\gamma}_n^2}{\overline{\lambda}_n^2}+\frac{1}{\overline{\lambda}_n^3}+1\right)\right)\right]\\&+\frac{1}{\overline{\lambda}_n\overline{\gamma}_p}\frac{\partial^2\widehat{\Phi}}{\partial\overline{\lambda}_n\partial\overline{\gamma}_p}\left[G_{12}-\frac{G_{23}}{\overline{\lambda}_n^2}+2G_{22}\left(\frac{\overline{\gamma}_n^2}{\overline{\lambda}_n^2}+\frac{1}{\overline{\lambda}_n^3}+1\right)\right]+\frac{G_{22}}{\overline{\lambda}_n^2}\left(\frac{\partial^2\widehat{\Phi}}{\partial\overline{\lambda}_n^2}-\frac{1}{\overline{\lambda}_n}\frac{\partial\widehat{\Phi}}{\partial\overline{\lambda}_n}\right)+\frac{E_2}{\overline{\lambda}_n}\frac{\partial\widehat{\Phi}}{\partial\overline{\lambda}_n}\\&+\frac{1}{\overline{\gamma}_p}\frac{\partial\widehat{\Phi}}{\partial\overline{\gamma}_p}\left[E_1-\frac{E_3}{\overline{\lambda}_n^2}+2\frac{G_{23}}{\overline{\lambda}_n^4}+\frac{G_{22}}{\overline{\lambda}_n^5}+\left(E_2-4\frac{G_{22}}{\overline{\lambda}_n^2}\right)\left(\frac{\overline{\gamma}_n^2}{\overline{\lambda}_n^2}+\frac{1}{\overline{\lambda}_n^3}+1\right)\right]\\&+\widetilde{\mu}\left[\frac{E_3}{\overline{\lambda}_n^2}-E_2\left(\frac{\overline{\gamma}_n^2}{\overline{\lambda}_n^2}+2\right)+\frac{2(2G_{22}(\overline{\gamma}_n^2+\overline{\lambda}_n^2)-G_{23})}{\overline{\lambda}_n^4}\right]>0,\end{aligned}\tag{21}$$

where it is recalled that the variables E_i, G_{1i}, G_{2i} and G_{3i} ($i=1,2,3$) are given by (19), and the partial derivatives of $\widehat{\Phi}$ with respect to $\overline{\lambda}_n$ and $\overline{\gamma}_p$ are known functions of $\overline{\lambda}_n$, $\overline{\gamma}_p$ and $\overline{\lambda}_1^{(2)}$, which, although much simpler than the corresponding derivatives of the more general estimate (6), are still too cumbersome to be included here.

The estimate of deBotton et al. for Neo-Hookean phases: Since the effective potentials (14) and (16) for composites with Neo-Hookean constituents differ only in their functional dependence on $\overline{\lambda}_n$ and $\overline{\gamma}_p$, the strong ellipticity condition for the deBotton et al. model may be readily obtained from (21) by explicit computation of the partial derivatives of expression (16) for $\widehat{\Phi}$ with respect to $\overline{\lambda}_n$ and $\overline{\gamma}_p$. The result can be shown to reduce to

$$\widetilde{\mu}\mathbf{v}\cdot\overline{\mathbf{B}}\mathbf{v}+\frac{\overline{\mu}-\widetilde{\mu}}{\overline{\lambda}_n}[(\overline{\lambda}_n^3-1)(\mathbf{n}\cdot\mathbf{v})^2+3(\mathbf{n}\cdot\mathbf{v})^2(\mathbf{n}\cdot\mathbf{u})^2]>0,\tag{22}$$

where it is recalled again that $\overline{\mu}$ and $\widetilde{\mu}$ are given explicitly by relations (12) and (13), respectively. It should be emphasized that the simplicity of condition (22), compared to (21), is due to the fact that for the deBotton et al. (2006) model (16) the three modes of shear are completely decoupled and the in-plane and antiplane responses are identical, while for the estimate (14) of Agoras et al. (2008) this is *not* true. The significance of these features on the development of macroscopic instabilities will be examined in Section 6 for uniaxial tension perpendicular to the fiber direction.

4. Aligned loadings

We are now in a position to examine the above-described conditions of strong ellipticity and determine subsequently the onset of macroscopic instabilities for the class of fiber-reinforced nonlinearly elastic materials described in Section 2, when subjected to *arbitrary*, *three-dimensional*, *finite deformations*. As already remarked in the preceding section, conditions (18), (21), and (22) are expected to hold true in small neighborhoods of $\overline{\mathbf{F}}=\mathbf{I}$ (i.e., for small enough deformations). But as the deformation progresses beyond $\overline{\mathbf{F}}=\mathbf{I}$ into the finite-deformation regime, a point may be reached at which their LHS vanish for some critical $\overline{\mathbf{F}}_{cr}$ and pair of critical vectors $\mathbf{v}_{cr}$ and $\mathbf{u}_{cr}$. The objective of this and of the next section is to compute the set of all such critical deformations ($\overline{\mathbf{F}}_{cr}$), and associated critical vectors ($\mathbf{v}_{cr}$ and $\mathbf{u}_{cr}$), in order to map out the complete onset of macroscopic instabilities in fiber-reinforced nonlinearly elastic materials under arbitrary finite deformations. In general, the computation of deformations $\overline{\mathbf{F}}_{cr}$ and vectors $\mathbf{v}_{cr}$ and $\mathbf{u}_{cr}$ for which the LHS of (18) and (21) vanish requires a tedious, but straightforward, numerical treatment. There are special loading paths, however, for which it is possible to

compute $\overline{\mathbf{F}}_{cr}$, $\mathbf{v}_{cr}$, and $\mathbf{u}_{cr}$ in closed form. On the other hand, because of its simpler structure, the computation of critical deformations $\overline{\mathbf{F}}_{cr}$ and critical vectors $\mathbf{v}_{cr}$ and $\mathbf{u}_{cr}$ for which the LHS of condition (22) ceases to be positive can be carried out analytically for arbitrary loading conditions.

In this section, we provide closed-form expressions for the critical deformations and critical stresses at which the estimates (6), (14), and (16) lose strong ellipticity under *aligned* axisymmetric and pure shear loading conditions. The results will be compared with the results of Rosen (1965) and Triantafyllidis and Maker (1985) for 2-D laminates. Corresponding results for more general loadings will be given in Sections 5 and 6.

For definiteness and without loss of generality, in this and the remaining sections, we will consider the initial direction of the fibers to be given by $\mathbf{N}=\mathbf{e}_3$, where $\{\mathbf{e}_i\}$ stands for the Cartesian basis utilized for the laboratory frame of reference (see Fig. 1(a)).

4.1. Axisymmetric shear

In this subsection, we generate explicit results for the onset of macroscopic instabilities in fiber-reinforced nonlinearly elastic materials—as characterized by the failure of the strong ellipticity conditions (18), (21), and (22)—subjected to axisymmetric macroscopic deformation gradients of the form

$$\overline{\mathbf{F}}=\overline{\lambda}^{-1/2}\mathbf{e}_1\otimes\mathbf{e}_1+\overline{\lambda}^{-1/2}\mathbf{e}_2\otimes\mathbf{e}_2+\overline{\lambda}\mathbf{e}_3\otimes\mathbf{e}_3. \tag{23}$$

After recognizing from (23) that $\overline{\lambda}_n=\overline{\lambda}$ and $\overline{\gamma}_n=\overline{\gamma}_p=0$ and some algebraic manipulation, it follows that the critical stretch, $\overline{\lambda}_{cr}$, at which the strong ellipticity condition (18) is violated under deformations of the form (23) is simply given by

$$\overline{\lambda}_{cr}=\left[\frac{(1-c_0)c_0(g^{(1)}_{\overline{I}_{cr}}-g^{(2)}_{\overline{I}_{cr}})^2}{((1-c_0)g^{(1)}_{\overline{I}_{cr}}+c_0g^{(2)}_{\overline{I}_{cr}})((1+c_0)g^{(1)}_{\overline{I}_{cr}}+(1-c_0)g^{(2)}_{\overline{I}_{cr}})}\right]^{1/3}, \tag{24}$$

where $g^{(r)}_{\overline{I}_{cr}}=dg^{(r)}(\overline{I}_{cr})/dI$ with $\overline{I}_{cr}=\overline{\lambda}^2_{cr}+2\overline{\lambda}^{-1}_{cr}$. In the physically relevant context when $g^{(1)}$ and $g^{(2)}$ are convex functions of their argument, it is easy to verify that the RHS of (24) is positive and less than one so that necessarily $\overline{\lambda}_{cr}<1$. That is, under axisymmetric shear deformations, macroscopic instabilities may occur only for *compressive* loadings in the fiber direction and *not* for tensile ones, which is in agreement with physical experience. Note further that (24) constitutes a nonlinear algebraic equation for $\overline{\lambda}_{cr}$ which—although trivially solvable by numerical means—may or may not be solvable in closed form depending on the functional character of $g^{(1)}$ and $g^{(2)}$. In particular, for Neo-Hookean phases (4)—and more generally for Gent phases (3) with $J^{(1)}_m=J^{(2)}_m$—Eq. (24) can be readily solved in closed form rendering

$$\overline{\lambda}_{cr}=\left[\frac{(1-c_0)c_0(\mu^{(1)}-\mu^{(2)})^2}{((1-c_0)\mu^{(1)}+c_0\mu^{(2)})((1+c_0)\mu^{(1)}+(1-c_0)\mu^{(2)})}\right]^{1/3}. \tag{25}$$

It is useful to note that this last expression may be rewritten more compactly as follows:

$$\overline{\lambda}_{cr}=\left(1-\frac{\widetilde{\mu}}{\overline{\mu}}\right)^{1/3}, \tag{26}$$

where it is recalled that $\widetilde{\mu}$ and $\overline{\mu}$ are, respectively, the longitudinal and axisymmetric shear moduli of the composite (in the linearized regime), and are given by relations (13) and (12). Thus, $\widetilde{\mu}$ characterizes the effective response of the fiber-reinforced material in *antiplane shear*, corresponding to a *soft* mode of deformation, while $\overline{\mu}$ characterizes the effective response in *axisymmetric shear*, corresponding to a *hard* mode. It is evident from this expression that a heterogeneity contrast $t=\mu^{(2)}/\mu^{(1)}\neq 1$ (e.g., stiffer fibers) is required for $\overline{\lambda}_{cr}$ to be finite (different from zero), and that $\overline{\lambda}_{cr}$ tends to 1 (i.e., the instability tends to happen earlier) as the fibers become stiffer.

The associated pair of critical vectors for which loss of strong ellipticity occurs at the critical stretch (24) are $\mathbf{v}_{cr}=\mathbf{e}_3$ and $\mathbf{u}_{cr}=\mathrm{Span}\{\mathbf{e}_1,\mathbf{e}_2\}$ (see Fig. 2(b)). In other words, under axisymmetric *compressive* deformations of the form (23) with $\overline{\lambda}<1$, fiber-reinforced materials become unstable because their overall shear response in *all* directions within the transverse plane to the fibers vanish identically. This result is consistent with the experimental results of Jelf and Fleck (1992) for reinforced elastomers (see also Fleck, 1997; Kyriakides and Ruff, 1997 for other materials capable of undergoing plastic deformation), which have revealed that the failure mode in fiber-reinforced composites subjected to *compressive* deformation in the fiber direction leads to kink band instabilities.

For completeness, the instability results presented above in *deformation space* are presented next in *stress space*. With a suitable choice of the arbitrary pressure associated with the macroscopic incompressibility constraint ($\det\overline{\mathbf{F}}=1$), the axisymmetric shear deformation (23) can equivalently be identified with a uniaxial stress condition (aligned with the direction of the fibers) of the form

$$\overline{\mathbf{S}}=\frac{\partial\widehat{W}}{\partial\overline{\mathbf{F}}}-p\overline{\mathbf{F}}^{-T}=\overline{S}_{33}(\overline{\lambda})\mathbf{e}_3\otimes\mathbf{e}_3. \tag{27}$$

Here, $\overline{\mathbf{S}}$ denotes the first Piola–Kirchhoff stress tensor and p stands for the Lagrange multiplier associated with the incompressibility constraint. In this context, it then follows that the critical (first Piola–Kirchhoff) stress in the fiber

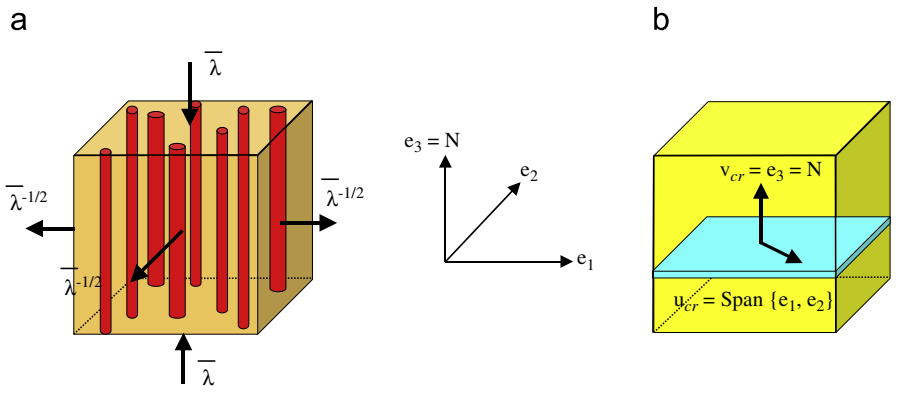

Fig. 2. (a) Schematic of a fiber-reinforced material subjected to aligned axisymmetric shear. (b) Illustration of the critical pair of orthogonal vectors, $\mathbf{v}_{cr}$ and $\mathbf{u}_{cr}$, for which the overall response of the material loses strong ellipticity.

direction at which the estimate (6) loses strong ellipticity under uniaxial stress is given by

$$\overline{S}_{cr} = \overline{S}_{33}(\overline{\lambda}_{cr}) = \frac{d\widehat{\Psi}}{d\overline{\lambda}}(\overline{\lambda}_{cr}) = 2(\overline{\lambda}_{cr} - \overline{\lambda}_{cr}^{-2})[(1-c_0)g_{\tilde{I}_{cr}}^{(1)} + c_0 g_{\tilde{I}_{cr}}^{(2)}], \tag{28}$$

where $\widehat{\Psi}(\overline{\lambda}) \doteq \widehat{\Phi}(\overline{\lambda}, 0, 0)$ and $\overline{\lambda}_{cr}$ is the critical stretch defined by (24). For the special case of Neo-Hookean phases, (28) can be shown to simplify to the compact form

$$\overline{S}_{cr} = -\widetilde{\mu}\left(\frac{\overline{\mu}}{\overline{\mu} - \widetilde{\mu}}\right)^{2/3}. \tag{29}$$

The physical significance of the expressions (26) and (29) will be discussed further in Section 4.4, where comparisons will also be made with the commonly used laminate (2-D) idealization for fiber-reinforced composites.

Having examined the condition (18) associated with the general estimate (6), we now turn attention to the strong ellipticity condition (22) associated with the Neo-Hookean estimate (16) of deBotton et al. (2006). In this connection, it is a simple matter to deduce that—under axisymmetric shear loadings of the form (23) with (27)—the LHS of (22) vanishes at the critical stretch (25) and critical vectors $\mathbf{v}_{cr} = \mathbf{e}_3$ and $\mathbf{u}_{cr} = \text{Span}\{\mathbf{e}_1, \mathbf{e}_2\}$, precisely as the LHS of (18) when specialized to Neo-Hookean phases.[1] Moreover, it is straightforward to show that the corresponding critical stress at which estimate (16) loses strong ellipticity is given by expression (29). That is, both homogenization estimates, (14) and (16), predict *exactly the same* critical deformation and the same critical stress for the onset of macroscopic instabilities in Neo-Hookean fiber-reinforced materials subjected to aligned axisymmetric shear.

With the objective of gaining more physical insight into the above-presented criteria for the onset of macroscopic instabilities, we develop further the above results for fiber-reinforced materials with Neo-Hookean (4) and Gent (3) matrix and fiber phases as functions of the (fiber-to-matrix) heterogeneity contrast $t = \mu^{(2)}/\mu^{(1)}$, volume fraction of fibers c_0, and lock-up parameters $J_m^{(1)}$ and $J_m^{(2)}$.

Fig. 3 presents results (labeled AXS) for the critical stretch (25) and stress (29) at which a fiber-reinforced material with Neo-Hookean matrix and fiber phases becomes macroscopically unstable when subjected to aligned axisymmetric shear loading (27) with (23). (Other results are shown in this figure for comparison and will be discussed in later sections.) Fig. 3(a) depicts the critical stretch $\overline{\lambda}_{cr}$ for a value of the fiber-to-matrix contrast $t = 20$, as a function of the volume fraction of fibers c_0. The main observation in this figure is that $\overline{\lambda}_{cr} \to 0$ as $c_0 \to 0$ and 1. This is consistent with the fact that both the pure matrix and fiber phases have been assumed to be strongly elliptic, so that in the absence of fibers ($c_0 = 0$) or matrix ($c_0 = 1$) the overall response remains stable for all deformations. As the initial volume fraction of fibers c_0 is increased from zero, $\overline{\lambda}_{cr}$ increases monotonically up to a certain $c_0 \leq 0.5$ at which it reaches a maximum. After this point, further increase in c_0 results in a monotonic decrease of $\overline{\lambda}_{cr}$. For fixed volume fraction of fibers (e.g., $c_0 = 0.3$), it can be seen from Fig. 3(b) that the critical stretch $\overline{\lambda}_{cr}$ increases monotonically with increasing fiber-to-matrix contrast t. In other words, the stiffer the behavior of the fibers (when compared to that of the matrix), the smaller the critical compressive deformation at which the fiber-reinforced material becomes unstable. In this regard, it is relevant to note that $\overline{\lambda}_{cr} \to 1$ as $t \to \infty$, irrespectively of the volume fraction of fibers (see expression (35) in Section 4.3). That is, in the limiting case of rigid fibers, the composite becomes unstable at zero strain (but not at zero stress of course). Similar observations can be made from Fig. 3(c) and (d) for the critical stress $\overline{S}_{cr}$. However, the maximum (i.e., smallest compressive value) for $\overline{S}_{cr}$ is skewed towards smaller fiber concentrations c_0, although $\overline{S}_{cr} \to -\infty$ as $c_0 \to 0$ and as $c_0 \to 1$, in line with the behavior observed in Fig. 3(a) for the

[1] The form (25) of the result was first presented by Lopez-Pamies and Ponte Castañeda (2006c), while the form (26) was first given by deBotton (2008).

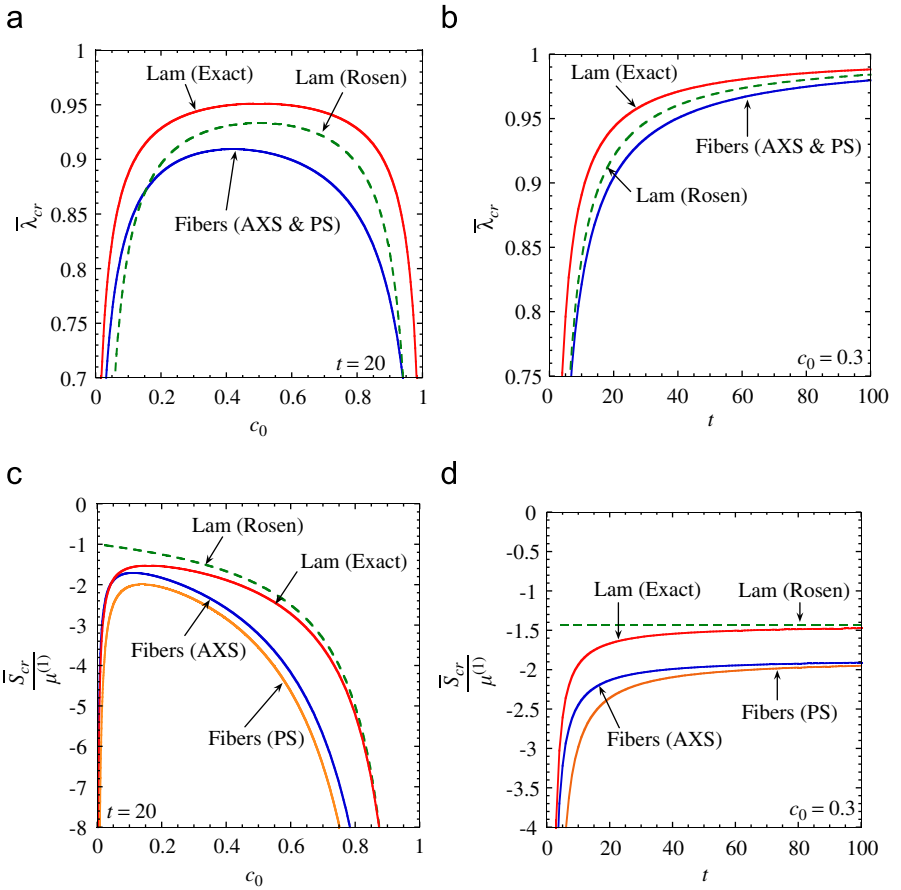

Fig. 3. Onset of macroscopic instabilities in fiber-reinforced materials with Neo-Hookean matrix and fiber phases subjected to *aligned axisymmetric shear* (AXS) and *pure shear* (PS) loading conditions. The critical stretch $\overline{\lambda}_{cr}$ (a) for fiber-to-matrix contrasts $t = \mu^{(2)}/\mu^{(1)} = 20$, as a function of the volume fraction of fibers c_0, and (b) for $c_0 = 0.3$, as a function of t. The critical stress $\overline{S}_{cr}$, normalized by $\mu^{(1)}$, corresponding to (a) and (b) are shown in (c) and (d), respectively. These results are compared with the *approximate* result of Rosen (1965), and the *exact* result of Triantafyllidis and Maker (1985) for laminates (Lam) under aligned pure shear.

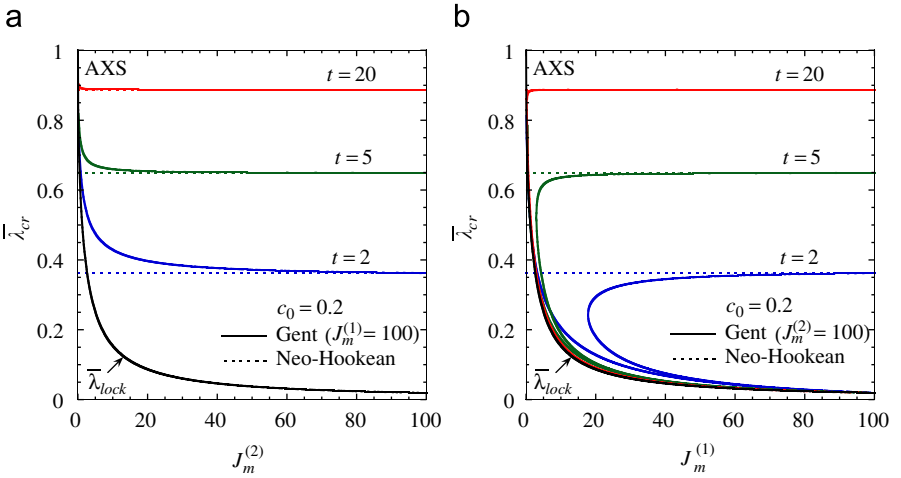

Fig. 4. Onset of macroscopic instabilities in fiber-reinforced materials with Gent phases subjected to *aligned axisymmetric shear* deformations (23), as given by expression (24). Results are shown for fiber-to-matrix contrasts $t = \mu^{(2)}/\mu^{(1)} = 2, 5, 20$, and volume fraction of the fibers $c_0 = 0.2$. (a) The critical stretch $\overline{\lambda}_{cr}$ for a fixed value of the lock-up parameter of the matrix, $J_m^{(1)} = 100$, as a function of $J_m^{(2)}$. (b) The critical stretch $\overline{\lambda}_{cr}$ for a fixed value of $J_m^{(2)} = 100$, as a function of $J_m^{(1)}$.

critical stretch. In addition, in the limit as the fibers are taken to be rigid (i.e., $t \to \infty$), the critical stress tends to a *non-zero* value, which for this volume fraction ($c_0 = 0.3$) is about twice the shear modulus of the matrix phase.

Fig. 4 illustrates the influence of the lock-up parameters of the matrix ($J_m^{(1)}$) and fibers ($J_m^{(2)}$) on the critical stretch (24) for fiber-reinforced materials with Gent phases, when subjected to aligned axisymmetric shear loadings (23). Results are shown for three values of the "initial" fiber-to-matrix contrast, $t = 2, 5, 20$, and volume fraction of the fibers $c_0 = 0.2$. Part (a) presents the critical stretch $\overline{\lambda}_{cr}$ for $J_m^{(1)} = 100$ as a function of $J_m^{(2)}$, and part (b) shows $\overline{\lambda}_{cr}$ for $J_m^{(2)} = 100$ as a function of $J_m^{(1)}$. The associated lock-up limit $\overline{\lambda}_{lock}$ for these materials, given by $\overline{\lambda}_{lock}^2 + 2/\overline{\lambda}_{lock} - 3 = \min\{J_m^{(1)}, J_m^{(2)}\}$ (see Section 5 in Agoras et al., 2008 for details), as well as the critical stretches for the corresponding composites with Neo-Hookean phases (i.e., $J_m^{(1)} = J_m^{(2)} = \infty$) have been included in this figure for comparison purposes. Note that the different branches of the curves shown in Fig. 4(b) correspond to distinct solutions of the *nonlinear* equation (24) for $\overline{\lambda}_{cr}$. It should be emphasized, however, that starting from the undeformed configuration and following the given axisymmetric loading path, the critical stretch at which a certain material becomes unstable corresponds to the highest among these values of $\overline{\lambda}_{cr}$. It is observed that for sufficiently large values of $J_m^{(2)}$ in part (a) and $J_m^{(1)}$ in part (b), these parameters have no essential effect on the stability of the composite and the associated critical stretch $\overline{\lambda}_{cr}$ is practically determined by the value of the contrast t. This observation is consistent with the fact that Gent materials behave like Neo-Hookean materials for deformations away from the lock-up limit $\overline{\lambda}_{lock}$. On the other hand, from part (a), we see that for small values of $J_m^{(2)}$ composites with Gent phases are more unstable than the corresponding composites with Neo-Hookean phases, while from part (b) we observe that for small values of $J_m^{(1)}$ the opposite is true. Recalling that for aligned axisymmetric shear (23) the deformation gradient field is uniform in the matrix and fibers (see He et al., 2006 and Section 4.1 in Agoras et al., 2008), these results may be understood as follows. For the case when $J_m^{(2)} < J_m^{(1)}$ (part (a)), as the applied stretch $\overline{\lambda}$ approaches the lock-up limit $\overline{\lambda}_{lock}$, the fibers tend to stiffen faster than the matrix with the consequence of effectively increasing the heterogeneity contrast (from its initial value $t = \mu^{(2)}/\mu^{(1)} > 1$) and thus accelerating the instability, while the opposite is true for $J_m^{(1)} < J_m^{(2)}$ (part (b)) (at least for not too small values of $J_m^{(1)}$, after which the behavior is controlled by the lock-up phenomenon).

4.2. Pure shear

Next, we consider the development of macroscopic instabilities for pure shear loadings of the form

$$\overline{\mathbf{F}} = \overline{\lambda}^{-1}\mathbf{e}_1 \otimes \mathbf{e}_1 + \mathbf{e}_2 \otimes \mathbf{e}_2 + \overline{\lambda}\mathbf{e}_3 \otimes \mathbf{e}_3, \tag{30}$$

where, similar to the preceding axisymmetric case, $\overline{\lambda}$ is a positive loading parameter, and it is recalled that the fibers are aligned in the $\mathbf{e}_3$ direction.

For the Neo-Hookean estimate (16) of deBotton et al. (2006), it is not difficult to show that when specialized to loading conditions of the form (30), the LHS of relation (22) vanishes at the critical stretch (26) and critical vectors $\mathbf{v}_{cr} = \mathbf{e}_3$ and $\mathbf{u}_{cr} = \mathrm{Span}\{\mathbf{e}_1, \mathbf{e}_2\}$ (see Fig. 2(b)). Thus, under *compressive* pure shear deformations of the form (30) with $\overline{\lambda} < 1$, fiber-reinforced materials become unstable because their overall shear response in *all* directions within the transverse plane to the fibers vanish identically. This is essentially the same "failure" mechanism that was observed in the preceding subsection for axisymmetric shear conditions.

Next, by suitably selecting the arbitrary hydrostatic pressure associated with the macroscopic incompressibility constraint, we can identify the pure shear deformation (30) with the following biaxial stress state

$$\overline{\mathbf{S}} = \overline{S}_{22}(\overline{\lambda})\mathbf{e}_2 \otimes \mathbf{e}_2 + \overline{S}_{33}(\overline{\lambda})\mathbf{e}_3 \otimes \mathbf{e}_3. \tag{31}$$

It follows that the critical stress along the fiber direction at which the estimate (16) loses strong ellipticity is given by

$$\overline{S}_{cr} = \overline{S}_{33}(\overline{\lambda}_{cr}) = -\widetilde{\mu}\frac{\overline{\mu}}{\overline{\mu} - \widetilde{\mu}}, \tag{32}$$

which is very similar (but not identical) to the corresponding result (29) for axisymmetric loading conditions.

It should also be noted that the corresponding estimates for the critical stretch and stress using the model of Agoras et al. (2008) may be easily computed for general behaviors for the phases. However, when specialized to the particular case of Neo-Hookean matrix and fiber phases (cf. (14)), the resulting estimates for the critical stretch and stress are very well approximated by expressions (26) and (32), respectively. Thus—as for axisymmetric shear—both homogenization estimates (14) and (16) predict *essentially the same* critical deformations and stresses for the onset of macroscopic instabilities for Neo-Hookean fiber-reinforced materials subjected to aligned pure shear. Sample results, labeled PS, for the case of Neo-Hookean constituents are shown in Fig. 3 as functions of the fiber volume fraction c_0 and contrast t. Comparing the results for $\overline{S}_{cr}$ for pure shear loading with the corresponding results for axisymmetric shear, it can be seen that the general trends are very similar. There are noticeable differences only for low values of the contrast t, but the differences tend to disappear as the contrast increases.

4.3. Asymptotic results in the limit of rigid fibers

The above-presented results correspond to general heterogeneity contrast between the matrix and the fibers. In practice, however, actual fibers in reinforced soft materials are usually several orders of magnitude stiffer than the matrix

phase. In this regard, it is convenient to spell out the specialization of the above results in the limit as the fibers are taken to be rigid. To this end, it is first helpful to recognize that the assumed smoothness and proper linearization of $g^{(1)}$ imply that

$$g^{(1)}(I) = \frac{\mu^{(1)}}{2}(I-3) + \frac{1}{2}g^{(1)}_{II}(3)(I-3)^2 + O((I-3)^3). \tag{33}$$

Then, by setting (without loss of generality)

$$g^{(2)}(I) = \frac{\mu^{(2)}}{2}(I-3) \tag{34}$$

and subsequently defining the fiber-to-matrix heterogeneity contrast $t = \mu^{(2)}/\mu^{(1)}$, it follows that expression (24) for the critical stretch at which instabilities develop for the case of *aligned axisymmetric shear loading conditions* reduces to

$$\overline{\lambda}_{cr} = 1 - \frac{1+c_0}{3(1-c_0)c_0}t^{-1} + O(t^{-2}), \tag{35}$$

in the limit as $t \to \infty$, namely, in the limit as the fibers are taken to be rigid. Expression (28) for the corresponding critical stress can be shown to specialize to

$$\overline{S}_{cr} = -\frac{1+c_0}{1-c_0}\mu^{(1)} + O(t^{-1}). \tag{36}$$

Interestingly, the critical stretch and stress at which instabilities develop for the case of *pure shear loading conditions* can also be shown to reduce to expressions (35) and (36), respectively, in the limit as $t \to \infty$. That is, in the limit of rigid fibers, the critical stretch $\overline{\lambda}_{cr}$ and critical stress $\overline{S}_{cr}$ for aligned axisymmetric shear deformations agree identically with the critical stretch $\overline{\lambda}_{cr}$ and critical stress $\overline{S}_{cr}$ for aligned pure shear deformations.

Moreover, it should be emphasized that the critical relations (35) and (36) are valid for materials with arbitrary generalized Neo-Hookean matrix behavior $g^{(1)}$, but because of the rigidity of the fibers, only the shear modulus in the ground state, $2g^{(1)}_I(3) = \mu^{(1)}$, enters these expressions. A practical implication of this result is that when considering the compressive failure in fiber-reinforced nonlinearly elastic materials with very stiff fibers, it suffices to model the matrix phase as Neo-Hookean. However, it should also be emphasized that the above asymptotic results tacitly assume that material parameters other than t are held fixed. As we have already seen, for instance, in the context of Fig. 4 for composites with Gent phases, how stiff the fibers need to be may depend on the values of the lock-up parameters of the matrix and fiber phases.

4.4. Comparisons with earlier results for laminates under pure shear loading

A popular strategy in the literature to estimate the compressive failure of fiber-reinforced composites has been to idealize these materials as laminates. The motivation for this simplifying approach stems from the fact that—under plane-strain loading conditions—laminates resemble 2-D fiber-reinforced morphologies (see Fig. 1(b)) and, at the same time, they permit an *exact* analytical treatment (see Appendix A for exact results for laminates with Neo-Hookean phases). In this section, we investigate the validity of such an approximation in light of the new results developed above for pure shear loading.

In one of the very first works proposing the use of laminates as 2-D approximations for fiber-reinforced composites, Rosen (1965) considered a perfect laminate made up of alternating layers of different *linear elastic* isotropic materials that is subjected to *plane-strain* compressive load along the layers. By means of an energy method, he solved the problem *approximately* and concluded that the critical stretch $\overline{\lambda}^{Ros}_{cr}$ and associated critical stress $\overline{S}^{Ros}_{cr}$ at which long-wavelength instabilities develop in these material systems are given by

$$\overline{\lambda}^{Ros}_{cr} = 1 - \frac{\mu^{(1)}}{3c_0(1-c_0)\mu^{(2)}} \quad \text{and} \quad \overline{S}^{Ros}_{cr} = -\frac{\mu^{(1)}}{1-c_0}. \tag{37}$$

Later, Triantafyllidis and Maker (1985) re-examined the laminate problem within the more general framework of finite elasticity. Specifically, these authors considered a perfect laminate, made up of alternating incompressible Neo-Hookean layers, under aligned pure shear loading conditions (30). By making use of Floquet theory for ODEs, they showed that the critical stretch $\overline{\lambda}^{L}_{cr}$ and associated critical stress $\overline{S}^{L}_{cr}$ at which long-wavelength instabilities develop in this case are given *exactly* by

$$\overline{\lambda}^{L}_{cr} = \left(1 - \frac{\widetilde{\mu}^{L}}{\overline{\mu}}\right)^{1/4} \quad \text{and} \quad \overline{S}^{L}_{cr} = -\widetilde{\mu}^{L}\left(\frac{\overline{\mu}}{\overline{\mu}-\widetilde{\mu}^{L}}\right)^{3/4}, \tag{38}$$

where $\overline{\mu}$ and $\widetilde{\mu}^{L}$ are defined by expressions (12) and $(62)_2$, respectively, and physically correspond to the "hard" axisymmetric (and transverse) shear mode and the "soft" longitudinal mode for small strains (see Appendix A). Note that the *exact* results (38) of Triantafyllidis and Maker are generally different from the *approximate* results (37) of Rosen; in particular, $\overline{\lambda}^{Ros}_{cr} \leq \overline{\lambda}^{L}_{cr}$ and $\overline{S}^{Ros}_{cr} \geq \overline{S}^{L}_{cr}$. However, both sets of results share the same physically expected qualitative features. Namely, they predict that long-wavelength instabilities occur only for compressive deformations (i.e., $\overline{\lambda}^{Ros}_{cr}, \overline{\lambda}^{L}_{cr} \leq 1$ and $\overline{S}^{Ros}_{cr}$,

$\overline{S}^{L}_{cr} \leq 0$). Moreover, both critical stretches, $\overline{\lambda}^{Ros}_{cr}$ and $\overline{\lambda}^{L}_{cr}$, are symmetric functions of the volume fractions of the matrix $1-c_0$ and of the fibers c_0, as a result of the symmetric role that the matrix and fiber constituents play in laminates (see Fig. 3 and the relevant discussion further below).

In connection with the above results for laminates, it is interesting to remark that the expressions (26), (29), and (32) for Neo-Hookean fiber-reinforced materials exhibit the same structure as the expressions (38) for Neo-Hookean laminates. In particular, both sets of results establish that long-wavelength instabilities may develop under aligned loadings whenever the compressive stretch in the fiber or layer direction reaches a critical value depending on the ratio of the "soft" effective longitudinal shear modulus to the "hard" axisymmetric shear modulus. (The differences in the exponents in these expressions are due to the different loadings and microstructures involved, since the relations between the stress and stretch variables are different for different loading conditions, e.g., pure shear vs. axisymmetric shear, while the response of layered and fiber-reinforced microstructures are also different.) More specific comparisons are given in Fig. 3, showing plots of $\overline{\lambda}_{cr}$ and $\overline{S}_{cr}$, as functions of the volume fraction of fibers c_0 and the fiber-to-matrix contrast $t=\mu^{(2)}/\mu^{(1)}$. Thus, it is observed from Fig. 3(a) and (b) that the critical stretch (26) for the axisymmetric and pure shear loading conditions (which, as already discussed, are identical to each other) indeed exhibit the same *qualitative* behavior as the exact critical stretch $(38)_1$ for laminates, both in terms of the dependence on volume fraction c_0, as well as contrast t. It is worth remarking, however, that unlike $(38)_1$, (26) is not symmetric about $c_0=0.5$. This feature is consistent with the fact that, unlike in laminates, the fibers and matrix phases in fiber-reinforced materials do *not* play a symmetric role. From a *quantitative* point of view, it is also observed that laminates are more unstable than fiber-reinforced materials, since they may develop long-wavelength instabilities at smaller compressive deformations (i.e., larger $\overline{\lambda}_{cr}$). Fig. 3(c) and (d) show that the critical stresses (29) and (32) for axisymmetric and pure shear loading conditions (which, as opposed to the associated stretches (26) are different from each other) are also in relatively good *qualitative* agreement with the corresponding exact result $(38)_2$ for laminates. Moreover, as in stretch-space, laminates are seen to be more unstable in stress-space than fiber-reinforced materials. It is also interesting to point out that for all results $\overline{\lambda}_{cr}\to 1$ in the limit of rigid fibers ($t\to\infty$). On the other hand, as $t\to\infty$, the stresses for laminates are seen to asymptotically approach a non-zero compressive value that is significantly smaller than that for fiber-reinforced materials.

5. Non-aligned loadings

Section 4 has provided some insight into the development of macroscopic instabilities in fiber-reinforced nonlinearly elastic materials subjected to *aligned* (axisymmetric and pure shear) loading conditions. In this section, we consider more general applied deformations in which the principal axes of loading are *not* aligned with the fiber direction. These include axisymmetric, pure, and simple shear at an angle relative to the fiber orientation **N**. Motivated by the fact that in realistic fiber-reinforced materials the underlying fibers are several orders of magnitude stiffer than the elastomeric matrix phase, we will primarily focus (see Section 4.3) on material systems with Neo-Hookean constituents, and take advantage of the model of deBotton et al. (2006) allowing for a full analytical treatment. However, some representative numerical results will also be presented using the model of Agoras et al. (2008) for materials with Gent phases in order to illustrate the differences that may arise for materials with *non-Neo-Hookean* matrix and fiber behaviors, especially when the critical deformations happen to be relatively large.

5.1. Axisymmetric shear at an angle

We start out by considering the case in which a fiber-reinforced nonlinearly elastic material is subjected to axisymmetric shear deformations of the form

$$\overline{\mathbf{F}}=\overline{\mathbf{Q}}\,\overline{\mathbf{D}}\,\overline{\mathbf{Q}}^{T} \tag{39}$$

with

$$\overline{\mathbf{D}}=\overline{\lambda}^{-1/2}\mathbf{e}_1\otimes\mathbf{e}_1+\overline{\lambda}^{-1/2}\mathbf{e}_2\otimes\mathbf{e}_2+\overline{\lambda}\mathbf{e}_3\otimes\mathbf{e}_3 \tag{40}$$

and

$$\overline{\mathbf{Q}}=\cos\Theta(\mathbf{e}_1\otimes\mathbf{e}_1+\mathbf{e}_3\otimes\mathbf{e}_3)+\sin\Theta(\mathbf{e}_1\otimes\mathbf{e}_3-\mathbf{e}_3\otimes\mathbf{e}_1)+\mathbf{e}_2\otimes\mathbf{e}_2. \tag{41}$$

Here, we recall that the fibers are initially aligned in the $\mathbf{e}_3$ direction and remark that the scalars $\overline{\lambda}>0$ and Θ play the role of two independent loading parameters. Note that $\Theta=n\pi$ ($n\in\mathbb{Z}$) corresponds to the aligned case presented in Section 4.1.

After substituting expression (39), with (40) and (41), in condition (22), it is a simple matter to deduce that the critical stretches at which macroscopic instabilities may first develop along axisymmetric shear loading paths at an angle satisfy

$$\overline{\lambda}^{3}_{cr}\cos^2\Theta-\overline{\lambda}_{cr}\left(1-\frac{\widetilde{\mu}}{\overline{\mu}}\right)^{2/3}+\sin^2\Theta=0, \tag{42}$$

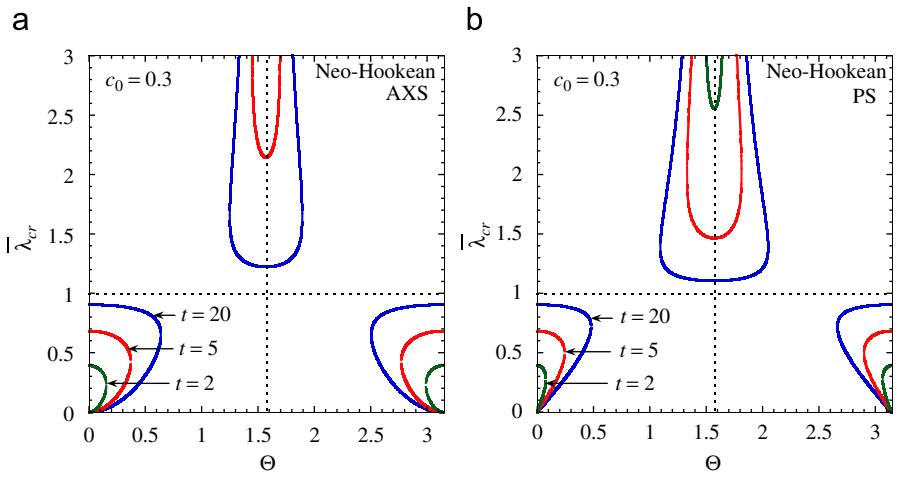

Fig. 5. Onset of macroscopic instabilities in fiber-reinforced materials with Neo-Hookean matrix and fiber phases subjected to *non-aligned* loadings: (a) *axisymmetric shear*, and (b) *pure shear*. The critical stretch $\overline{\lambda}_{cr}$ is shown for fiber-to-matrix contrasts $t = \mu^{(2)}/\mu^{(1)} = 2, 5, 20$, volume fraction of fibers $c_0 = 0.3$, as a function of the angle of fiber misalignment Θ.

while the associated critical vectors are given by $\mathbf{v}_{cr} = \cos\alpha_{cr}\mathbf{e}_1 + \sin\alpha_{cr}\mathbf{e}_3$ and $\mathbf{u}_{cr} = \mathbf{e}_2$, with $\tan\alpha_{cr} = (\cot\Theta)/(1-\overline{\lambda}_{cr}^{3/2}) + \overline{\lambda}_{cr}^{3/2}(\tan\Theta)/(1-\overline{\lambda}_{cr}^{3/2})$. As expected, Eq. (42) is periodic in Θ with period π. For the limiting values $\Theta = 0, \pi$ expression (42) reduces, of course, to (26).

To help examine the more general situation of intermediate values $\Theta \in (0, \pi)$, Fig. 5(a) provides plots for $\overline{\lambda}_{cr}$ as a function of Θ, for fiber-to-matrix contrasts $t = \mu^{(2)}/\mu^{(1)} = 2, 5, 20$ and volume fraction of fibers $c_0 = 0.3$. (Part (b) of this figure will be discussed in the context of the next subsection.) A key observation from Fig. 5(a) is that $\overline{\lambda}_{cr} < 1$ for angles near $\Theta = 0$ and $\Theta = \pi$, whereas $\overline{\lambda}_{cr} > 1$ for angles near $\Theta = \pi/2$. By contrast, there is a finite range of angles neighboring $\Theta = \pi/4$ and $\Theta = 3\pi/4$ for which macroscopic instabilities do not occur. Physically, these results entail that fiber-reinforced materials may develop macroscopic instabilities only when the deformation along the direction of the fibers is compressive and of a sufficiently large magnitude. Indeed, under loading conditions of the form (39) with $\overline{\lambda} < 1$, $\Theta = 0$ and $\Theta = \pi$ correspond to the cases at which maximum compression is applied along the fibers. Likewise, for $\overline{\lambda} > 1$ in (39), $\Theta = \pi/2$ corresponds to the case at which maximum compression is applied along the fibers. Deviating the value of Θ away from 0 and π when $\overline{\lambda} < 1$, and away from $\pi/2$ when $\overline{\lambda} > 1$, effectively decreases the amount of compression in the fiber direction, with the angles $\Theta = \pi/4$ and $\Theta = 3\pi/4$ corresponding to the cases in which the applied compressive deformation along the fibers is the smallest. In line with the findings of Section 4.1 for aligned axisymmetric loading conditions, Fig. 5(a) shows that increasing the heterogeneity contrast t results in macroscopic instabilities developing at smaller (tensile or compressive) deformations. In other words, the larger the contrast between the fibers and the matrix, the more unstable the behavior of fiber-reinforced materials becomes. Given the loading path independence proper of hyperelastic materials, it is seen from Fig. 5 that macroscopic instabilities may be possible at larger deformations for "non-radial" loading paths (i.e., when Θ is a function of $\overline{\lambda}$). In this case, the curves shown in Fig. 5 should be interpreted as macroscopic "failure surfaces" in the sense of Triantafyllidis et al. (2006).

5.2. Pure shear at an angle

We consider now the case in which a fiber-reinforced nonlinearly elastic material is subjected to pure shear deformations of the form (39) with $\overline{\mathbf{Q}}$ given by (41) and

$$\overline{\mathbf{D}} = \overline{\lambda}^{-1}\mathbf{e}_1 \otimes \mathbf{e}_1 + \mathbf{e}_2 \otimes \mathbf{e}_2 + \overline{\lambda}\mathbf{e}_3 \otimes \mathbf{e}_3. \tag{43}$$

Here, similar to the axisymmetric case, the scalars $\overline{\lambda} > 0$ and Θ are loading parameters. Note that $\Theta = n\pi$ $(n \in \mathbb{Z})$ corresponds to the aligned case presented in Section 4.2. Note further that the shifts $\overline{\lambda} \to \overline{\lambda}^{-1}$ and $\Theta \to \Theta + \pi/2$ lead to the same loading.

By making explicit use of expression (39), with (43) and (41), in the strong ellipticity condition (22), it follows that the critical stretch at which macroscopic instabilities may develop in this case is solution to the following quartic equation:

$$\overline{\lambda}_{cr}^4 \cos^2\Theta - \overline{\lambda}_{cr}^2\left(1 - \frac{\widetilde{\mu}}{\overline{\mu}}\right)^{2/3} + \sin^2\Theta = 0. \tag{44}$$

Moreover, the corresponding critical vectors can be shown to be given by $\mathbf{v}_{cr} = \cos\alpha_{cr}\mathbf{e}_1 + \sin\alpha_{cr}\mathbf{e}_3$ and $\mathbf{u}_{cr} = \mathbf{e}_2$, where the angle α_{cr} is defined by $\tan\alpha_{cr} = (\cot\Theta)/(1-\overline{\lambda}_{cr}^2) + \overline{\lambda}_{cr}^2(\tan\Theta)/(1-\overline{\lambda}_{cr}^2)$. Note that Eq. (44) is periodic in Θ with period π, and hence it is sufficient to examine values $\Theta \in [0, \pi]$. Note further that for $\Theta = 0, \pi$ expression (44) reduces, of course, to (26).

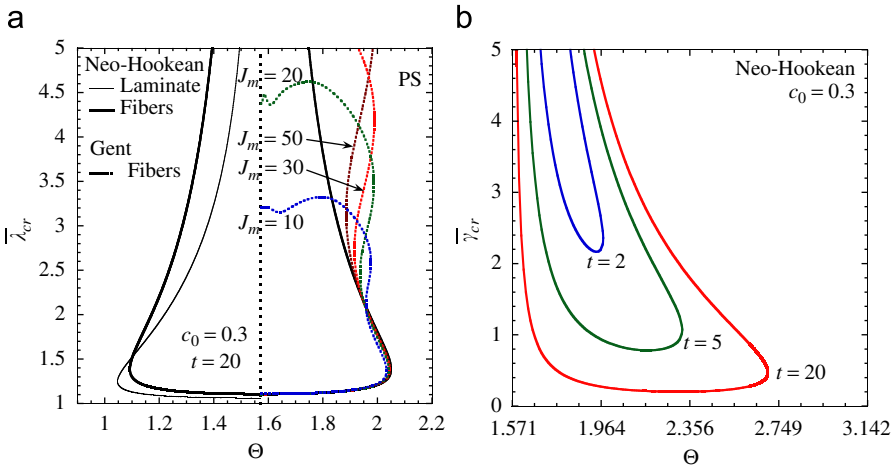

Fig. 6. Onset of macroscopic instabilities in fiber-reinforced materials subjected to *non-aligned* loadings. (a) Comparison of *pure shear* failure surfaces for a Neo-Hookean fiber-reinforced composite with Gent fiber-reinforced composites (right) and with a Neo-Hookean laminate (left). All material systems have $c_0 = 0.3$ and $t = 20$, while for materials with Gent phases results are shown for several values of J_m (10, 20, 30, 50). (b) The critical stretch $\overline{\gamma}_{cr}$ for Neo-Hookean matrix and fiber phases under *simple shear* loading, as a function of the fiber misalignment angle Θ, for $t = \mu^{(2)}/\mu^{(1)} = 2, 5, 20$, and $c_0 = 0.3$.

Fig. 5(b) presents macroscopic failure surfaces for fiber-to-matrix contrasts $t = \mu^{(2)}/\mu^{(1)} = 2, 5, 20$ and volume fraction of fibers $c_0 = 0.3$, and shows that the onset of macroscopic instabilities along non-aligned pure shear loading paths is similar in character to the onset of macroscopic instabilities for non-aligned axisymmetric shear deformations (cf. Fig. 5(a)). Indeed, it is observed that $\overline{\lambda}_{cr} < 1$ around $\Theta = 0$ and $\Theta = \pi$, $\overline{\lambda}_{cr} > 1$ around $\Theta = \pi/2$, and macroscopic instabilities do not occur near $\Theta = \pi/4$ and $\Theta = 3\pi/4$. Again, these results imply that fiber-reinforced materials may develop macroscopic instabilities only when the deformation along the direction of the fibers is of a sufficiently large compressive magnitude. Moreover, increasing the contrast t (and the volume fraction of fibers c_0, although not shown) is seen to render fiber-reinforced materials more unstable, irrespectively of the angle of fiber misalignment Θ.

The right side of Fig. 6(a) shows a comparison of the failure surfaces for fiber-reinforced materials with Gent phases, with lock-up values $J_m^{(1)} = J_m^{(2)} = J_m = 10, 20, 30$ and 50, with the corresponding surfaces for fiber-reinforced materials with Neo-Hookean phases ($J_m \to \infty$) for $t = 20$ and $c_0 = 0.3$. In the context of Fig. 6(a), it should be noted that the lower branches displayed in Fig. 5(b) are exactly equivalent to the upper branch, when account is made of the invariance of the equations under the transformations $\overline{\lambda} \to \overline{\lambda}^{-1}$ and $\Theta \to \Theta + \pi/2$. For this reason, in Fig. 6(a) only the upper branch is shown (magnified). In addition, only the right half of the Gent failure surfaces are shown, given their symmetry about the vertical axis. It can be seen from this figure that while the Neo-Hookean failure surfaces close up at infinity, the Gent surfaces close at a finite value of the stretch $\overline{\lambda}$, depending on the lock-up parameter J_m. However, for "radial" loading paths (i.e., for constant Θ) these differences are not relevant since the Gent and Neo-Hookean fiber composites are seen to fail at similar values of $\overline{\lambda}$, thus giving credence to the explicit formula (44) for materials other than Neo-Hookean.

For *non-aligned*, but still plane-strain, loading conditions, it is also possible to compute (in closed form) the exact critical deformations at which macroscopic instabilities may develop in Neo-Hookean laminates; the result is given by expression (65) in Appendix A. The predictions are qualitatively very similar (although quantitatively different) to the predictions for fiber-reinforced materials discussed earlier. An illustration of this is provided in Fig. 6(a) for pure shear at an angle (refer to the left side of the graph). There, it can be seen that the exact results for a laminate with Neo-Hookean phases—as given by expression (66) in Appendix A—are quite similar to the predictions for the fiber-reinforced material also with Neo-Hookean phases—as given by expression (44). Thus, these results indicate that modeling the behavior of fiber-reinforced nonlinearly elastic materials as laminates is certainly appropriate—in *qualitative* terms—when restricting attention to the special case of *plane-strain* loading conditions. As elaborated in Section 6, however, this is not true when considering more general three-dimensional (3-D) loading conditions.

5.3. Simple shear at an angle

Next, we consider applied simple shear deformations of the form (39), where now

$$\overline{\mathbf{D}} = \mathbf{I} - \overline{\gamma}\mathbf{e}_1 \otimes \mathbf{e}_3 \tag{45}$$

with $\overline{\gamma} \geq 0$ and Θ being two independent loading parameters. Under this type of loading conditions, the critical amount of shear, $\overline{\gamma}_{cr}$, at which condition (22) first fails can be shown to be solution to the following quadratic equation:

$$\overline{\gamma}_{cr}^2 \frac{1 + \cos 2\Theta}{2} + \overline{\gamma}_{cr} \sin 2\Theta - \left(1 - \frac{\widetilde{\mu}}{\overline{\mu}}\right)^{2/3} + 1 = 0, \tag{46}$$

while the associated critical vectors can be shown to be given by $\mathbf{v}_{cr} = \cos\alpha_{cr}\mathbf{e}_1 + \sin\alpha_{cr}\mathbf{e}_3$ and $\mathbf{u}_{cr} = \mathbf{e}_2$ with $\tan\alpha_{cr} = \cot\Theta - (\csc\Theta)^2/\overline{\gamma}_{cr}$. Again, as expected, Eq. (46) is periodic in Θ with period π, and therefore we restrict attention to the domain $\Theta \in [0,\pi]$. After recalling the inequality $\overline{\mu} \geq \widetilde{\mu}$, it is straightforward to check that within the range $\Theta \in [0,\pi/2]$, there is no real positive $\overline{\gamma}_{cr}$ that satisfies (46). On the contrary, for $\Theta \in (\pi/2,\pi)$, there are finite positive values of $\overline{\gamma}_{cr}$ for which Eq. (46) is satisfied.

Fig. 6(b) shows a few of these results for $\overline{\gamma}_{cr}$, as a function of Θ, for $t = 2, 5, 20$ and $c_0 = 0.3$. It is noted that these failure surfaces look like shifted and distorted versions of the corresponding surfaces in Fig. 6(a), the reason for this being that the loading (45) actually corresponds to the pure shear loading (43), together with a superposed rotation (which also depends on $\overline{\gamma}$). It is interesting that this applied rotation now makes "accessible" the previously unaccessible left side of the failure surface for pure shear (for a radial path). Similar to all previous cases, Fig. 6(b) shows that for all values of fiber misalignment Θ, increasing the fiber-to-matrix contrast t and volume fraction of fibers c_0 (in the range of values considered) also render fiber-reinforced materials more unstable when subjected to non-aligned simple shear deformations. In addition, although not explicitly illustrated in the plots, Fig. 6(b) does show that $\overline{\gamma}_{cr}$ is smaller for angles Θ for which more compressive deformation is applied along the direction of the fibers.

6. General loading conditions

By means of specific cases, Sections 4 and 5 have revealed that fiber-reinforced nonlinearly elastic materials can develop long-wavelength instabilities when subjected to loading conditions enforcing a sufficiently large compressive deformation along the fiber direction. In Section 6.1, we consider completely general loading conditions and cast the generic conclusions of the previous subsections for materials with Neo-Hookean constituents in general form using, for simplicity, the model of deBotton et al. (2006). The relevance of this explicit result for more general material behavior will be explored in Section 6.2 in the context of transverse uniaxial tension loading, where comparisons will also be made with the 2-D laminate approximation, showing the inappropriateness of this approximation for general loading conditions.

6.1. A closed-form analytical result for general loadings

As demonstrated in Appendix B, given an arbitrary loading path with starting point $\overline{\mathbf{F}} = \mathbf{I}$, the critical deformation gradient, $\overline{\mathbf{F}}_{cr}$, at which condition (22) first ceases to hold true is determined by the *invariant* expression

$$(\overline{\mathbf{F}}_{cr}\mathbf{N})\cdot(\overline{\mathbf{F}}_{cr}\mathbf{N}) = \|\overline{\mathbf{F}}_{cr}\mathbf{N}\|^2 = \left(1 - \frac{\widetilde{\mu}}{\overline{\mu}}\right)^{2/3}. \tag{47}$$

This relation states quite simply that fiber-reinforced hyperelastic materials may develop long-wavelength instabilities whenever the stretch in the fiber direction $\overline{\lambda}_n = \|\overline{\mathbf{F}}\mathbf{N}\|$ reaches a certain critical value depending on the antiplane-to-axisymmetric ratio of the ground shear moduli $\widetilde{\mu}/\overline{\mu}$.

The corresponding critical vectors $\mathbf{v}_{cr}$ and $\mathbf{u}_{cr}$ for which condition (22) fails are given by

$$\mathbf{v}_{cr} = \|\overline{\mathbf{F}}_{cr}^{-T}\mathbf{N}\|^{-1}\overline{\mathbf{F}}_{cr}^{-T}\mathbf{N} \tag{48}$$

and

$$\mathbf{u}_{cr} = \|(\overline{\mathbf{F}}_{cr}\mathbf{N})\times(\overline{\mathbf{F}}_{cr}^{-T}\mathbf{N})\|^{-1}(\overline{\mathbf{F}}_{cr}\mathbf{N})\times(\overline{\mathbf{F}}_{cr}^{-T}\mathbf{N}), \tag{49}$$

respectively. Interestingly, the vector (48) is seen to correspond to the image (in the deformed configuration) of $\mathbf{N}$ when treated not as a material line element, but as the normal to a material surface element. Furthermore, note that the vector (49) is perpendicular to the direction of the fibers in the deformed configuration, $\mathbf{n} = \|\overline{\mathbf{F}}_{cr}\mathbf{N}\|^{-1}\overline{\mathbf{F}}_{cr}\mathbf{N}$, and, of course, also perpendicular to (48), as a result of the macroscopic incompressibility constraint.

It is also of interest to note here that the corresponding critical stress at which condition (22) fails is given by

$$\overline{\mathbf{S}}_{cr} = \widetilde{\mu}\overline{\mathbf{F}}_{cr}(\mathbf{I} - \mathbf{N}\otimes\mathbf{N}) + \left[\overline{\mu}\left(1 - \frac{\widetilde{\mu}}{\overline{\mu}}\right)^{2/3} - p\right]\overline{\mathbf{F}}_{cr}^{-T}, \tag{50}$$

where p is the Lagrange multiplier associated with the incompressibility constraint, and $\overline{\mathbf{F}}_{cr}$ is (partially) determined by condition (47).

It should be emphasized that these results are rigorously valid for the model of deBotton et al. (2006) for fiber-reinforced composites with Neo-Hookean phases. However, as we have seen in the preceding sections (see in particular Section 4.3), the result (47) for the critical deformation should also provide a good approximation not just for fiber-reinforced materials with Neo-Hookean phases, but more generally for fiber-reinforced materials with any incompressible, isotropic, nonlinearly elastic constituents, provided that the fibers are sufficiently stiffer than the matrix phase (and therefore the resulting critical deformations are not too large). On the other hand, as it will be seen in the next subsection, the result (50) for the corresponding critical stress $\overline{\mathbf{S}}_{cr}$ is not expected to hold for general constitutive behavior for the phases, since it is clear from the derivation that this result will be highly dependent on the assumed behavior of the matrix and fibers.

6.2. Transverse uniaxial tension

We conclude this section with one final example involving general 3-D loading conditions. Referring to Fig. 1(a), we consider *transverse uniaxial tension* (perpendicular to the fiber direction) of the form

$$\overline{\mathbf{S}} = \frac{\partial \widehat{W}}{\partial \overline{\mathbf{F}}} - p\overline{\mathbf{F}}^{-T} = \overline{S}(\overline{\lambda})\mathbf{e}_1 \otimes \mathbf{e}_1. \tag{51}$$

Given the transverse isotropy of the fiber-reinforced material, this type of stress loading condition leads to a triaxial deformation with macroscopic gradient

$$\overline{\mathbf{F}} = \overline{\lambda}\mathbf{e}_1 \otimes \mathbf{e}_1 + (\overline{\lambda}\,\overline{\lambda}_n)^{-1}\mathbf{e}_2 \otimes \mathbf{e}_2 + \overline{\lambda}_n\mathbf{e}_3 \otimes \mathbf{e}_3, \tag{52}$$

where the loading parameter $\overline{\lambda}$ corresponds to the stretch in the loading direction ($\mathbf{e}_1$) and $\overline{\lambda}_n$ denotes the stretch along the fiber direction ($\mathbf{e}_3$). For constitutive relations of the form $\widehat{W}(\overline{\mathbf{F}}) = \widehat{\Phi}(\overline{\lambda}_n, \overline{\gamma}_p, \overline{\gamma}_n)$, it is a simple matter to deduce that $\overline{\lambda}_n$ in (52) must satisfy the relation

$$\frac{\partial \widehat{\Phi}}{\partial \overline{\lambda}_n}(\overline{\lambda}_n, \overline{\lambda} - (\overline{\lambda}\,\overline{\lambda}_n)^{-1}, 0) + \frac{1}{\overline{\lambda}\,\overline{\lambda}_n^2}\frac{\partial \widehat{\Phi}}{\partial \overline{\gamma}_p}(\overline{\lambda}_n, \overline{\lambda} - (\overline{\lambda}\,\overline{\lambda}_n)^{-1}, 0) = 0. \tag{53}$$

Moreover, the tensile stress $\overline{S}$ in (51) satisfies the following identity:

$$\overline{S}(\overline{\lambda}) = \left(1 + \frac{1}{\overline{\lambda}^2\overline{\lambda}_n}\right)\frac{\partial \widehat{\Phi}}{\partial \overline{\gamma}_p}(\overline{\lambda}_n, \overline{\lambda} - (\overline{\lambda}\,\overline{\lambda}_n)^{-1}, 0). \tag{54}$$

Under the transverse tension loading (51), the strong ellipticity condition (18) associated with the model of Agoras et al. (2008) can be shown to first fail whenever $\overline{\lambda}$ and $\overline{\lambda}_n$ reach critical values, $1 < \overline{\lambda}_{cr} < \infty$, and $0 < \overline{\lambda}_n^{cr} \leq 1$, that satisfying the nonlinear equation

$$\overline{\lambda}_{cr}^2\frac{\partial^2 \widehat{\Phi}}{\partial \overline{\gamma}_n^2}(\overline{\lambda}_n^{cr}, \overline{\lambda}_{cr} - (\overline{\lambda}_{cr}\overline{\lambda}_n^{cr})^{-1}, 0) - [\overline{\lambda}_{cr} + (\overline{\lambda}_{cr}\overline{\lambda}_n^{cr})^{-1}]\frac{\partial \widehat{\Phi}}{\partial \overline{\gamma}_p}(\overline{\lambda}_n^{cr}, \overline{\lambda}_{cr} - (\overline{\lambda}_{cr}\overline{\lambda}_n^{cr})^{-1}, 0) = 0, \tag{55}$$

where it is emphasized that $\overline{\lambda}$ and $\overline{\lambda}_n$ are related by relation (53); the associated critical vectors are given by $\mathbf{v}_{cr} = \mathbf{e}_3$ and $\mathbf{u}_{cr} = \mathbf{e}_1$. Moreover, the corresponding critical stress is simply given by relation (54) evaluated at $\overline{\lambda}_{cr}$, namely $\overline{S}_{cr} = \overline{S}(\overline{\lambda}_{cr})$.

Unfortunately, the nonlinear, algebraic, coupled equations (53) and (55) for $\overline{\lambda}_{cr}$ and $\overline{\lambda}_n^{cr}$ do not admit significant simplification and, in general, must be treated numerically. However, for the special case of a Neo-Hookean matrix reinforced with rigid fibers, we have that $\overline{\lambda}_n = 1$, and the above critical conditions reduce to the following equation for $\overline{\lambda}_{cr}$:

$$\overline{\lambda}_{cr}^4 - 2(\overline{\lambda}_{cr}^3 - \overline{\lambda}_{cr} + 1) = c_0^{-1}, \tag{56}$$

which may be shown to have a *finite* root such that $1 < \overline{\lambda}_{cr} < \infty$, implying, in turn, a finite (positive) value for $\overline{S}_{cr}$. In this connection, it is interesting to note that when the fibers are rigid, the deformation is essentially plane-strain (transverse) shear. This case has already been discussed by Lopez-Pamies and Ponte Castañeda (2006b) as a 2-D plane-strain problem, and no (in-plane) macroscopic instabilities were found (for fibers with circular cross-sections). The above result is not inconsistent with the earlier finding, because in the present analysis, we are considering the possibility of more general 3-D bifurcations (that are not consistent with the plane-strain assumption).

The conditions (52)–(55), of course, also hold for the model of deBotton et al. (2006). In this case, the expression (16) for the effective stored-energy function $\widehat{\Phi}$ is completely explicit, so that its derivatives can be computed explicitly. It can then be readily seen that the first and second terms in expression (55) cancel out, so that the expression for the loss of ellipticity under transverse uniaxial loading conditions (51) reduces to

$$(\overline{\lambda}_{cr}\overline{\lambda}_n^{cr})^{-2}\widetilde{\mu} = 0, \tag{57}$$

which can only be achieved (asymptotically) in the limit as $\overline{\lambda} \to \infty$. This implies that the critical condition (47) for $\overline{\lambda}_n$ is only reached asymptotically for infinite $\overline{\lambda}$, and therefore, from expression (54), that the corresponding critical stress $\overline{S}_{cr}$ is unbounded. Thus, the model of deBotton et al. (2006) gives the prediction that *no* macroscopic instability is expected for this type of stress loading condition, in stark contradiction with the corresponding predictions arising from the model of Agoras et al. (2008). The fundamental reason for this difference can be traced to the different predictions of the two models for the transverse shear response. As already noted, the model of deBotton et al. (2006) exhibits the same response for longitudinal and transverse shear, while the model of Agoras et al. (2008) exhibits a different response for these two modes, with the transverse shear mode being stiffer. Although the differences are small, recent numerical results by Moraleda et al. (2009) do appear to confirm the stiffer predictions of the model of Agoras et al. (2008) for transverse shear, strongly suggesting the possible development of macroscopic instabilities in transverse tension. Of course, only experiments can ultimately determine whether macroscopic instabilities can occur for this type of loading condition, but regardless of the outcome this example demonstrates just how sensitive these instabilities can be to the accuracy of the constitutive model on which they are based.

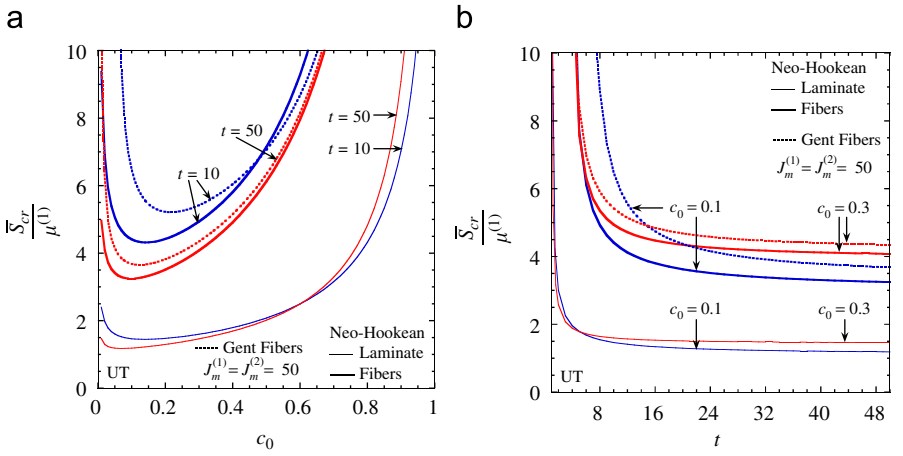

Fig. 7. Comparison of the predictions for macroscopic instabilities under transverse uniaxial tensile (UT) loading for fiber-reinforced (with both Gent and Neo-Hookean phases) and laminates (with Neo-Hookean phases). The critical stress $\overline{S}_{cr}$, normalized by the shear modulus of the matrix phase $\mu^{(1)}$, for (a) fiber-to-matrix contrasts $t = \mu^{(2)}/\mu^{(1)} = 10, 50$, as a function of the volume fraction of fibers c_0, and for (b) $c_0 = 0.1, 0.3$, as a function of t.

Next, for comparison purposes, we consider the predictions for the laminate model (60) for Neo-Hookean phases (see Appendix A), when subjected to the uniaxial loading condition (51). Referring to Fig. 1(b), we note that this loading condition corresponds to uniaxial tension perpendicular to the layers. In this case, the resulting deformation is transversely isotropic of the form $\overline{\mathbf{F}} = \overline{\lambda}\mathbf{e}_1 \otimes \mathbf{e}_1 + \overline{\lambda}^{-1/2}\mathbf{e}_2 \otimes \mathbf{e}_2 + \overline{\lambda}^{-1/2}\mathbf{e}_3 \otimes \mathbf{e}_3$, where the tensile stretch $\overline{\lambda}$ is related to the applied stress via

$$\overline{S}(\overline{\lambda}) = (\overline{\lambda} - \overline{\lambda}^{-2})\overline{\mu}. \tag{58}$$

The corresponding critical stretch and stress for the onset of macroscopic instabilities is determined via expression (64) (see Appendix A), which leads to the results

$$\overline{\lambda}_{cr}^{L} = \left(1 - \frac{\widetilde{\mu}^{L}}{\overline{\mu}}\right)^{-1/3} \quad \text{and} \quad \overline{S}_{cr}^{L} = \widetilde{\mu}^{L}\left(\frac{\overline{\mu}}{\overline{\mu} - \widetilde{\mu}^{L}}\right)^{1/3}, \tag{59}$$

respectively. Here, it is recalled that the moduli $\widetilde{\mu}^{L}$ and $\overline{\mu}$ have been defined in (62). In addition, it is noted that the critical vectors are given by $\mathbf{v}_{cr} = \text{Span}\{\mathbf{e}_2, \mathbf{e}_3\}$ and $\mathbf{u}_{cr} = \mathbf{e}_1$.

Fig. 7 presents a detailed comparison of the predictions for the critical stress $\overline{S}_{cr}$ of the laminate model (with Neo-Hookean phases) with the model of Agoras et al. (2008) for fiber-reinforced composites (with both Neo-Hookean and Gent phases), when subjected to transverse uniaxial loading. (Recall that the model of deBotton et al., 2006 predicts no instabilities for this loading.) The results for the laminate were obtained by means of expression $(59)_2$, while the results for the fiber-reinforced composites were obtained using expressions (54), along with (53) and (55). Part (a) shows plots of $\overline{S}_{cr}$, normalized by $\mu^{(1)}$, for fiber-to-matrix contrasts $t = \mu^{(2)}/\mu^{(1)} = 10, 50$, as a function of the fiber concentration c_0, while part (b) presents corresponding results for $c_0 = 0.1, 0.3$, as a function of t. In all plots, the value $J_m^{(1)} = J_m^{(2)} = 50$ has been used for the fiber composite with Gent constituents. The main observation from these results is that fiber-reinforced materials are substantially more stable than laminates for this loading. This result may be understood as follows. For the laminate, as discussed earlier, the deformation is transversely isotropic, and the applied stress leads to an equal amount of compressive stretch (i.e., hydrostatic deformation) in the plane of the stiff layers ($\mathbf{e}_2 - \mathbf{e}_3$), while for the fiber-reinforced composite, the applied tensile stress (perpendicular to the fibers) can be accommodated to a large extent by compressive deformation along the other direction ($\mathbf{e}_2$) perpendicular to the fibers, resulting in a proportionally smaller compressive stretch along the fiber direction ($\mathbf{e}_3$). It is also interesting to note that in the limit of infinite contrast $t \to \infty$ the laminate becomes macroscopically unstable at $\overline{\lambda}_{cr} = 1$, while for the fiber composite $\overline{\lambda}_{cr} > 1$ (compare (56) and $(59)_1$). In other words, a material reinforced with rigid fibers may accommodate some transverse deformation before failure, while the corresponding rigidly reinforced laminate cannot. Put together, these observations demonstrate that the laminate model does not provide reliable estimates for the onset of macroscopic instabilities in fiber-reinforced materials for general loading conditions.

In Section 6.1, use was made of the model of deBotton et al. (2006) to derive the expression (47) describing the onset of macroscopic instabilities in fiber-reinforced composites with Neo-Hookean phases. In addition, it was argued that this expression should also apply for fiber-reinforced composites with more general constitutive behaviors for the constituent phases, provided that the critical deformation $\overline{\mathbf{F}}_{cr}$ is not too large. However, we have found in this section that the model of deBotton et al. (2006) can lead to potentially inconsistent predictions for certain types of loading conditions. This raises the question as to the validity of the above proposal. To shed some light on this point, Fig. 8 presents a comparison of the

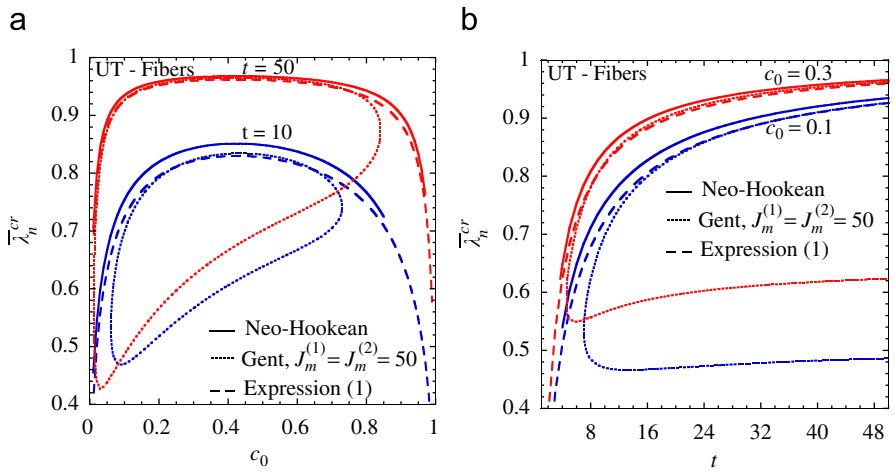

Fig. 8. Comparison of the predictions for macroscopic instabilities under transverse uniaxial tension (UT) for fiber-reinforced (with both Gent and Neo-Hookean phases) with the general analytical formula (1). The critical stretch $\overline{\lambda}_n^{cr}$ along the fiber direction for (a) fiber-to-matrix contrasts $t = \mu^{(2)}/\mu^{(1)} = 10, 50$, as a function of the volume fraction of fibers c_0, and for (b) $c_0 = 0.1, 0.3$, as a function of t.

instability predictions of the model of Agoras et al. (2008) for two different composites (one with Neo-Hookean phases and the other with Gent phases) with the analytical formula (47) for the critical value of the stretch $\overline{\lambda}_n^{cr}$ along the fiber direction under the uniaxial tensile loading (51). Parts (a) and (b) provide results for the same values of the parameters used in parts (a) and (b) of Fig. 7 for the corresponding critical stress $\overline{S}_{cr}$. (Results are not shown for the laminates, as we have already seen that these results are fundamentally inconsistent with the results for actual fiber-reinforced composites in this case.) The main observation is that the predictions of the Agoras et al. model, as described by expressions (53) and (55) for $\overline{\lambda}_{cr}$ and $\overline{\lambda}_n^{cr}$, are in relatively good agreement with the analytical formula (47) for $\overline{\lambda}_n^{cr}$, even though the agreement is actually quite poor for $\overline{\lambda}_{cr}$ (not shown). The main differences occur for the larger fiber concentrations, when the Gent composite tends to lock up at stretches that are smaller than the critical stretches predicted by the formula (47), due to the strain concentration in the matrix at these higher concentrations. However, as can be seen from Fig. 8(b), these differences in $\overline{\lambda}_n^{cr}$ improve with increasing fiber-to-matrix contrast $t = \mu^{(2)}/\mu^{(1)}$, and they practically disappear for sufficiently large values of t. On the other hand, it can be seen in Fig. 7(b) that the differences in the corresponding critical stresses for Neo-Hookean and Gent fiber composites are more significant and they tend to persist even at large contrast. Therefore, we conclude that the formula (47) for the critical value of the stretch $\overline{\lambda}_n^{cr}$ along the fiber direction can be safely used for general loading conditions and general material behavior, provided that the fibers are sufficiently stiffer than the matrix phase.

7. Concluding remarks

In this work, we presented a detailed study of the macroscopic failure of fiber-reinforced hyperelastic composites with random microstructures under general 3-D, finite-strain loading conditions. Based on the fundamental work of Geymonat et al. (1993), the onset of failure in these materials was identified with the development of long-wavelength instabilities, corresponding to the loss of strong ellipticity of their homogenized behavior. For the characterization of the effective response of these materials we utilized the recently developed model of Agoras et al. (2008), which applies to composites with a fairly general class of hyperelastic behavior for their constituent phases, as well as the model of deBotton et al. (2006), which is applicable only to composites with Neo-Hookean constituents. The influence of the local properties of the matrix and fibers and of the volume fraction of fibers on the development of macroscopic instabilities was discussed in detail for several loadings (both aligned and non-aligned with the microstructure), where such instabilities would be expected to occur from physical experience. These results show that the main parameters controlling the possible onset of macroscopic instabilities are the fiber-to-matrix heterogeneity contrast and the fiber volume fraction. On the other hand, the specific features of the constitutive behavior of the phases (e.g., the lock-up parameter J_m for a Gent material) are less important, but may have a significant effect for small-contrast systems. For the practically important class of materials in which the fibers are much stiffer than the matrix, it was found that expression (47) provides a very good approximation for the corresponding critical deformation gradient under general loading conditions. This formula is insensitive to the specific constitutive models used for the phases, and shows that macroscopic instabilities may develop in fiber-reinforced elastic composites when the stretch along fibers direction reaches a critical value determined only by the ratio of the longitudinal-to-axisymmetric effective shear moduli of the composite for infinitesimal strains. Furthermore, it was found that, by properly accounting for the differences between the transverse and longitudinal modes at large strain (Moraleda et al., 2009), the model of Agoras et al. (2008) appears to give more realistic predictions for the possible onset of instabilities than the corresponding model of deBotton et al. (2006). In particular, for the special case of uniaxial tensile stress transverse to

the fiber direction, the model of Agoras et al. (2008) gives a prediction consistent with the development of instabilities at a finite stress by virtue of the Poisson effect which leads to the activation of the critical condition (47) in the stretch along the fibers, while the model of deBotton et al. (2006) results in the prediction of no instability, as the critical condition (47) is only achieved asymptotically for an infinite tensile stress in the transverse direction. In this connection, it is important to note that while the model of Agoras et al. (2008) made use of a Walpole-type estimate for the pertinent "linear comparison composite," the "second-order" procedure on which it is based can be used to obtain more specific estimates for special classes of fiber-reinforced composites. Such estimates may exhibit different responses for the transverse and longitudinal modes, even in the range of infinitesimal deformations. For this reason, we propose here the generalization (1) of the analytical estimate (47) for composites with more general linearized behavior exhibiting different effective ground shear moduli for the transverse and longitudinal modes.

In this work, we also investigated the validity of 2-D laminate models that have been used extensively in the literature to study approximately the stability of fiber-reinforced composites. For plane-strain loadings, for which the laminates do resemble fiber-reinforced composites, fairly good qualitative (but less good quantitative) agreement was observed for the corresponding instability predictions for the two classes of composites. On the other hand, for more general 3-D loadings, including transverse uniaxial tension, the estimates based on the laminate model for the onset of macroscopic instabilities were found to deviate significantly from the corresponding estimates for real fiber-reinforced systems, showing that the use of laminate models for general 3-D loadings is not appropriate. We propose instead the use of the analytical formula (1) for the critical stretch along the fiber direction, along with the model of Agoras et al. (2008) for the macroscopic constitutive relation of the fiber-reinforced composites under general loading (including prescribed traction) conditions.

Finally, as revealed by an extensive body of literature on the compressive failure of fiber composites (see, e.g., Kyriakides and Ruff, 1997; Fleck, 1997), the presence of imperfections, in general, and of plasticity for many materials, can have a significant effect on the onset of macroscopic instabilities in fiber-reinforced composites. While the specific results developed in this work are limited to systems with perfectly elastic behavior for the phases and perfectly aligned fibers, the general methods from which they have been derived can be generalized to incorporate the effect of imperfections in the microstructure (see Lopez-Pamies et al., 2008 for an example in the context of oriented thermoplastic elastomers), as well as the effect of plasticity. The advantage of these potential extensions lies in the generality of the underlying framework, which is not restricted to specific loading conditions, or other simplifying hypotheses. Such generalizations will be pursued in future work.

Acknowledgments

This material is based upon work supported by the National Science Foundation under Grants CMMI-0654063 and DMS-0708271.

Appendix A. Exact results for the macroscopic behavior of Neo-Hookean laminates

As stated in the main body of the text, numerous works have proposed the use of laminates as 2-D approximations for fiber-reinforced composites because: (i) they resemble fiber-reinforced morphologies (compare Fig. 1(b) with Fig. 1(a)) and (ii) they permit, at the same time, an exact analytical treatment. With the objective of aiding the discussion of Section 6 about the validity of using laminates as approximations for fiber-reinforced nonlinearly elastic materials, in this appendix we summarize some *exact closed-form results* for laminates with (incompressible) Neo-Hookean phases of the form (4). Specifically, we provide results for the effective stored-energy function and the associated condition of strong ellipticity for *arbitrary 3-D finite deformations*. The pertinent derivations are a straightforward application of the framework given by Lopez-Pamies and Ponte Castañeda (2009) and thus will not be detailed here. Instead, we proceed directly with the presentation of the final relevant results.

The effective stored-energy function for a laminate with Neo-Hookean phases (4) and direction of lamination $\mathbf{N}$ (see Fig. 1(b)), subjected to a macroscopic deformation gradient $\overline{\mathbf{F}}$, can be shown to be given by

$$\widehat{W}(\overline{\mathbf{F}}) = \frac{\overline{\mu}}{2}(\overline{\mathbf{F}}\cdot\overline{\mathbf{F}} - 3) - \frac{\overline{\mu} - (\overline{\mu^{-1}})^{-1}}{2}[(\overline{\mathbf{F}}\mathbf{N})\cdot(\overline{\mathbf{F}}\mathbf{N}) - [(\overline{\mathbf{F}}^{-T}\mathbf{N})\cdot(\overline{\mathbf{F}}^{-T}\mathbf{N})]^{-1}]. \tag{60}$$

where $\overline{\mu}$ and $(\overline{\mu^{-1}})^{-1}$ denote the arithmetic and harmonic averages of $\mu^{(1)}$ and $\mu^{(2)}$ (see also deBotton, 2005 for a 2-D version of the result). This expression linearizes properly, as it reduces to the corresponding estimate in the limit as $\overline{\mathbf{F}} \to \mathbf{I}$, namely

$$\widehat{W}(\overline{\mathbf{F}}) = \frac{\widetilde{\mu}_a^L}{2}\overline{\varepsilon}_a^2 + \frac{\widetilde{\mu}_p^L}{2}\overline{\varepsilon}_p^2 + \frac{\widetilde{\mu}_n^L}{2}\overline{\varepsilon}_n^2 + O(\|\overline{\mathbf{F}} - \mathbf{I}\|^3), \tag{61}$$

where $\overline{\varepsilon}_a$, $\overline{\varepsilon}_p$, and $\overline{\varepsilon}_n$ are the axisymmetric, transverse, and longitudinal shear invariants of the infinitesimal strain tensor, which were introduced in the context of expression (11), and

$$\widetilde{\mu}_a^L = \widetilde{\mu}_p^L = \overline{\mu} \quad \text{and} \quad \widetilde{\mu}_n^L = (\overline{\mu^{-1}})^{-1} = \left(\frac{1-c_0}{\mu^{(1)}} + \frac{c_0}{\mu^{(2)}}\right)^{-1} \equiv \widetilde{\mu}^L. \tag{62}$$

Note that, as expected, relation (60) is a transversely isotropic scalar function of $\overline{\mathbf{F}}$ with symmetry axis $\mathbf{N}$. In terms of the canonical basis of transversely isotropic invariants $\bar{I}_1$, $\bar{I}_2$, $\bar{I}_4$, and $\bar{I}_5$, (60) can be rewritten as $\widehat{W}(\overline{\mathbf{F}}) = \widehat{\Psi}(\bar{I}_1, \bar{I}_2, \bar{I}_4, \bar{I}_5)$, where

$$\widehat{\Psi}(\bar{I}_1, \bar{I}_2, \bar{I}_4, \bar{I}_5) = \frac{\overline{\mu}}{2}(\bar{I}_1 - 3) - \frac{\overline{\mu} - \widetilde{\mu}^L}{2}[\bar{I}_4 - (\bar{I}_2 - \bar{I}_1\bar{I}_4 + \bar{I}_5)^{-1}]. \tag{63}$$

In connection with this expression, it is worth remarking that in spite of the fact that the underlying *local* Neo-Hookean behavior (4) does not depend on the second invariant I_2, the *macroscopic* behavior (63) does depend on $\bar{I}_2$. Moreover, it is interesting to note that the *exact* relation (63) is *not* of the simple separable form $W = W_{iso}(I_1, I_2) + W_{ani}(I_4, I_5)$, which has often been assumed in the literature (see, e.g., Horgan and Saccomandi, 2005 and references therein) on a purely phenomenological basis.

Next, we write down the condition of strong ellipticity (17), as specialized to the constitutive relation (60):

$$\overline{\mu}(\overline{\mathbf{F}}^T\mathbf{v})\cdot(\overline{\mathbf{F}}^T\mathbf{v}) - (\overline{\mu} - \widetilde{\mu}^L)[(\overline{\mathbf{F}}\mathbf{N})\cdot\mathbf{v}]^2 - (\overline{\mu} - \widetilde{\mu}^L)[(\overline{\mathbf{F}}^{-T}\mathbf{N})\cdot(\overline{\mathbf{F}}^{-T}\mathbf{N})]^{-2}[(\overline{\mathbf{F}}^{-T}\mathbf{N})\cdot\mathbf{u}]^2[1 - 4[(\overline{\mathbf{F}}^{-T}\mathbf{N})\cdot(\overline{\mathbf{F}}^{-T}\mathbf{N})]^{-1}[(\overline{\mathbf{F}}^{-T}\mathbf{N})\cdot\mathbf{v}]^2] > 0. \tag{64}$$

Here, it is recalled that the unit vectors $\mathbf{v}$ and $\mathbf{u}$ satisfy the incompressibility constraint $\mathbf{v}\cdot\mathbf{u} = 0$. For *plane-strain* loading conditions under which laminates resemble fiber-reinforced materials (i.e., in the context of Fig. 1(b), deformations in the $\mathbf{e}_1-\mathbf{e}_3$-plane), the critical deformation gradient $\overline{\mathbf{F}}_{cr}$ and corresponding critical vectors $\mathbf{v}_{cr}$ and $\mathbf{u}_{cr}$ at which condition (64) is first violated can be computed in closed form. The result for $\overline{\mathbf{F}}_{cr}$ reads as follows:

$$\frac{1 - [(\overline{\mathbf{F}}_{cr}^{-T}\mathbf{N})\cdot(\overline{\mathbf{F}}_{cr}^{-T}\mathbf{N})]^2}{[(\overline{\mathbf{F}}_{cr}^{-T}\mathbf{N})\cdot(\overline{\mathbf{F}}_{cr}^{-T}\mathbf{N})][(\overline{\mathbf{F}}_{cr}\mathbf{N})\cdot(\overline{\mathbf{F}}_{cr}\mathbf{N})]} = \frac{\widetilde{\mu}^L}{\overline{\mu}}. \tag{65}$$

It is relevant to remark that expression (65) generalizes the classical result $(38)_1$ of Triantafyllidis and Maker (1985) for *aligned* loading conditions, to general loading conditions. When the applied macroscopic deformation is parameterized (without loss of generality) as a pure shear at an angle $\overline{\mathbf{F}} = \overline{\mathbf{Q}}\,\overline{\mathbf{D}}\,\overline{\mathbf{Q}}^T$, with $\mathbf{N} = \mathbf{e}_3$ and $\overline{\mathbf{Q}}$ and $\overline{\mathbf{D}}$ given by (41) and (43), expression (65) takes the more explicit form

$$\overline{\lambda}_{cr}^8[\overline{\mu} + \widetilde{\mu}^L + (\overline{\mu} - \widetilde{\mu}^L)\cos 2\Theta]\cos^2\Theta - \overline{\lambda}_{cr}^4\frac{\overline{\mu} - \widetilde{\mu}^L}{2}(3 + \cos 4\Theta) + [\overline{\mu} + \widetilde{\mu}^L - (\overline{\mu} - \widetilde{\mu}^L)\cos 2\Theta]\sin^2\Theta = 0. \tag{66}$$

Note that for the particular case when $\Theta = 0$, relation (66) does indeed reduce to the classical result $(38)_1$ of Triantafyllidis and Maker (1985). Sample results for more general non-aligned loading conditions are shown in Fig. 6(a).

Appendix B. Demonstration of the criticality expressions (47)–(49)

In this appendix, we provide a demonstration of the criticality conditions (47)–(49) for the *first* loss of ellipticity in the expression (22) associated with the model of deBotton et al. (2006). To this end, we first show that the LHS of (22) does indeed vanish when evaluated at the values $\overline{\mathbf{F}}_{cr}$, $\mathbf{v}_{cr}$, and $\mathbf{u}_{cr}$ given by (47), (48), and (49). Then, we show that there are no macroscopic deformations smaller than those defined by (47) at which the LHS of (22) vanishes.

We start out by noticing that upon direct implementation of expressions (48) and (49),

$$\begin{aligned}
&\mathbf{v}_{cr}\cdot\overline{\mathbf{B}}\mathbf{v}_{cr} = \frac{1}{\|\overline{\mathbf{F}}_{cr}^{-T}\mathbf{N}\|^2}(\overline{\mathbf{F}}_{cr}^{-T}\mathbf{N})\cdot(\overline{\mathbf{F}}_{cr}\overline{\mathbf{F}}_{cr}^T\overline{\mathbf{F}}_{cr}^{-T}\mathbf{N}) = \frac{1}{\|\overline{\mathbf{F}}_{cr}^{-T}\mathbf{N}\|^2},\\
&\mathbf{n}\cdot\mathbf{v}_{cr} = \frac{1}{\overline{\lambda}_n\|\overline{\mathbf{F}}_{cr}^{-T}\mathbf{N}\|}(\overline{\mathbf{F}}_{cr}\mathbf{N})\cdot(\overline{\mathbf{F}}_{cr}^{-T}\mathbf{N}) = \frac{1}{\overline{\lambda}_n\|\overline{\mathbf{F}}_{cr}^{-T}\mathbf{N}\|},\\
&\mathbf{n}\cdot\mathbf{u}_{cr} = 0,
\end{aligned} \tag{67}$$

where it is recalled that the unit vector $\mathbf{N}$ characterizes the direction of the fibers in the undeformed configuration, and $\overline{\lambda}_n = \|\overline{\mathbf{F}}_{cr}\mathbf{N}\|$. Making explicit use of these results in condition (22) leads to

$$\|\overline{\mathbf{F}}_{cr}^{-T}\mathbf{N}\|^{-2}\left(\widetilde{\mu} + \frac{\overline{\mu} - \widetilde{\mu}}{\overline{\lambda}_n^3}[(\overline{\lambda}_n^3 - 1)]\right) > 0, \tag{68}$$

which is seen to be violated at the critical deformations defined by (47), when $\overline{\lambda}_n = (1 - \widetilde{\mu}/\overline{\mu})^{1/3}$.

Next, to show that condition (22) first fails at deformations defined by (47)—and *not* before—it proves helpful to define $\mathbf{v}^* = \overline{\mathbf{F}}^T\mathbf{v}$, $\mathbf{u}^* = \overline{\mathbf{F}}^T\mathbf{u}$, and to introduce the parametrization

$$\overline{\lambda}_n = \delta\left(1 - \frac{\widetilde{\mu}}{\overline{\mu}}\right)^{1/3}, \tag{69}$$

where δ is a positive parameter, such that $\overline{\lambda}_n > (1 - \widetilde{\mu}/\overline{\mu})^{1/3}$ whenever $\delta > 1$ (i.e., loss of ellipticity *earlier* than that given by condition (47) would correspond to a value of $\delta > 1$). Then, after some algebraic manipulation, the strong ellipticity condition (22) may be rewritten in the form

$$Q \equiv \widetilde{\mu}[\mathbf{v}^* \cdot \mathbf{v}^* - (\mathbf{N} \cdot \mathbf{v}^*)^2] + \overline{\mu}(\mathbf{N} \cdot \mathbf{v}^*)^2 \left[1 - \delta^{-3} + 3\delta^{-5}\left(1 - \frac{\widetilde{\mu}}{\overline{\mu}}\right)^{-2/3} (\mathbf{N} \cdot \mathbf{u}^*)^2\right] > 0. \tag{70}$$

Note that $\overline{\mu} \geq \widetilde{\mu} > 0$, $(\mathbf{N} \cdot \mathbf{u}^*)^2 \geq 0$, $\mathbf{v}^* \cdot \mathbf{v}^* > 0$, $(\mathbf{N} \cdot \mathbf{v}^*)^2 \geq 0$, and $\mathbf{v}^* \cdot \mathbf{v}^* - (\mathbf{N} \cdot \mathbf{v}^*)^2 \geq 0$. Clearly, these conditions ensure that $Q \geq 0$ when $\delta > 1$ (since $1 - \delta^{-3} > 0$ in this case). To show that $Q > 0$ whenever $\delta > 1$, we consider two mutually exclusive cases: (i) $\mathbf{v}^*$ is not aligned with $\mathbf{N}$ in which case the first term is strictly positive and the second is non-negative, so that $Q > 0$. (ii) $\mathbf{v}^*$ is parallel to $\mathbf{N}$ in which case the first term vanishes identically and the smallest value of the second term occurs when $\mathbf{u}^*$ is perpendicular to $\mathbf{N}$ so that $Q = \overline{\mu}(\mathbf{N} \cdot \mathbf{v}^*)^2(1 - \delta^{-3}) > 0$. Of course, when $\delta = 1$, case (ii) is exactly equivalent to the criticality conditions (47)–(49).

References

Abdelmoula, R., Krasucki, F., Marigo, J.-J., 1993. Microbuckling analysis of unidirectional fibred composites. In: Mecamat 93—International Seminar on Micromechanics of Materials. Collection de la Direction des Etudes et Recherches d'Electricité de France, Eyrolles, pp. 303–314.

Agoras, M., Lopez-Pamies, O., Ponte Castañeda, P., 2008. A general hyperelastic model for incompressible fiber-reinforced elastomers. Journal of the Mechanics and Physics of Solids 57, 268–286.

Brun, M., Lopez-Pamies, O., Ponte Castañeda, P., 2007. Homogenization estimates for fiber-reinforced elastomers with periodic microstructures. International Journal of Solids and Structures 44, 5953–5979.

deBotton, G., 2005. Transversely isotropic sequentially laminated composites in finite elasticity. Journal of the Mechanics and Physics of Solids 53, 1334–1361.

deBotton, G., 2008. Composites with one and two families of fibers. Presented at the Composites and Polycrystals Mini-Symposium at the 2008 SIAM Conference on Mathematical Aspects of Materials Science, Philadelphia.

deBotton, G., Hariton, I., Socolsky, E.A., 2006. Neo-Hookean fiber-reinforced composites in finite elasticity. Journal of the Mechanics and Physics of Solids 54, 533–559.

deBotton, G., Ponte Castañeda, P., 1993. Elastoplastic constitutive relations for fiber-reinforced solids. International Journal of Solids and Structures 30, 1865–1890.

Ericksen, J.L., Rivlin, R.S., 1954. Large elastic deformations of homogeneous anisotropic materials. Indiana University Mathematics Journal 3, 281–301.

Finlay, H.M., Whittaker, P., Canham, P.B., 1998. Collagen organization in branching region of human brain arteries. Stroke 29, 1595–1601.

Fleck, N., 1997. Compressive failure of fiber composites. Advances in Applied Mechanics 33, 43–117.

Gent, A.N., 1996. A new constitutive relation for rubber. Rubber Chemistry and Technology 69, 59–61.

Geymonat, G., Müller, S., Triantafyllidis, N., 1993. Homogenization of nonlinearly elastic materials, microscopic bifurcation and macroscopic loss of rank-one convexity. Archive for Rational Mechanics and Analysis 122, 231–290.

Grandidier, J.C., Poitier-Ferry, M., 1990. Fiber microbuckling in a long fiber composite material. Comptes Rendus de l'Academie des Sciences, Serie II 310, 1–6.

Guo, Z.Y., Peng, X.Q., Moran, B., 2006. A composites-based hyperelastic constitutive model for soft tissue with application to the human annulus fibrosus. Journal of the Mechanics and Physics of Solids 54, 1952–1971.

He, Q.C., Le Quang, H., Feng, Z.Q., 2006. Exact results for the homogenization of elastic fiber-reinforced solids at finite strain. Journal of Elasticity 83, 153–177.

Hill, R., 1972. On constitutive macrovariables for heterogeneous solids at finite strain. Proceedings of the Royal Society of London A 326, 131–147.

Holzapfel, G.A., Gasser, T.C., Ogden, R.W., 2000. A new constitutive framework for arterial wall mechanics and a comparative study of material models. Journal of Elasticity 61, 1–48.

Honeker, C.C., Thomas, E.L., 1996. Impact of morphological orientation in determining mechanical properties in triblock copolymers. Chemistry of Materials 8, 1702–1714.

Honeker, C.C., Thomas, E.L., Albalak, R.J., Hadjuk, D.A., Gruner, S.M., Capel, M.C., 2000. Perpendicular deformation of a near-single crystal triblock copolymer with a cylindrical morphology. 1. Synchrotron SAXS. Macromolecules 33, 9395–9406.

Horgan, C.O., Saccomandi, G., 2005. A new constitutive theory for fiber-reinforced incompressible nonlinearly elastic solids. Journal of the Mechanics and Physics of Solids 53, 1985–2015.

Jelf, P.M., Fleck, N., 1992. Compression failure mechanisms in unidirectional composites. Journal of Composite Materials 26, 2706–2726.

Kyriakides, S., Ruff, A.E., 1997. Aspects of the failure and postfailure of fiber composites in compression. Journal of Composite Materials 31, 1633–1670.

Lopez-Pamies, O., Garcia, R., Chabert, E., Cavaillé, J.-Y., Ponte Castañeda, P., 2008. Multiscale modeling of oriented thermoplastic elastomers with lamellar morphology. Journal of the Mechanics and Physics of Solids 56, 3206–3223.

Lopez-Pamies, O., Ponte Castañeda, P., 2006a. On the overall behavior, microstructure evolution, and macroscopic stability in reinforced rubbers at large deformations: I—Theory. Journal of the Mechanics and Physics of Solids 54, 807–830.

Lopez-Pamies, O., Ponte Castañeda, P., 2006b. On the overall behavior, microstructure evolution, and macroscopic stability in reinforced rubbers at large deformations: II—Application to cylindrical fibers. Journal of the Mechanics and Physics of Solids 54, 831–863.

Lopez-Pamies, O., Ponte Castañeda, P., 2006c. Effective behavior, microstructure evolution and macroscopic instabilities in reinforced elastomers. Presented at the Instabilities in Solids, Structures and Materials Mini-Symposium at the 15th U.S. National Congress of Theoretical and Applied Mechanics, Boulder.

Lopez-Pamies, O., Ponte Castañeda, P., 2009. Microstructure evolution in hyperelastic laminates and implications for overall behavior and macroscopic stability. Mechanics of Materials 41, 364–374.

Merodio, J., Ogden, R.W., 2003. Instabilities and loss of ellipticity in fiber-reinforced nonlinearly elastic solids under plane deformation. International Journal of Solids and Structures 40, 4707–4727.

Merodio, J., Ogden, R.W., 2005. Mechanical response of fiber-reinforced incompressible nonlinear elastic solids. International Journal of Nonlinear Mechanics 40, 213–227.

Merodio, J., Pence, T.J., 2001. Kink surfaces in a directionally reinforced Neo-Hookean material under plane deformation: I. Mechanical equilibrium. Journal of Elasticity 62, 119–144.

Michel, J.-C., Lopez-Pamies, O., Ponte Castañeda, P., Triantafyllidis, N., 2009. Microscopic and macroscopic instabilities in finitely strained reinforced elastomers, in preparation.

Moraleda, J., Segurado, J., Llorca, J., 2009. Computational micromechanics of fiber-reinforced elastomers. Journal of the Mechanics and Physics of Solids 57, 1596–1613.

Nesterovic, N., Triantafyllidis, N., 2004. Onset of failure in finitely strained layered composites subjected to combined normal and shear loading. Journal of the Mechanics and Physics of Solids 52, 941–974.

Ogden, R., 1984. Non-linear Elastic Deformations. Dover Publications, New York.

Ogden, R., 1978. Extremum principles in non-linear elasticity and their application to composites—I. Theory. International Journal of Solids and Structures 14, 265–282.

Ponte Castañeda, P., 1989. The overall constitutive behavior of nonlinearly elastic composites. Proceedings of the Royal Society of London A 422, 147–171.

Ponte Castañeda, P., 1996. Exact second-order estimates for the effective mechanical properties of nonlinear composite materials. Journal of the Mechanics and Physics of Solids 44, 827–862.
Ponte Castañeda, P., 2002. Second-order homogenization estimates for nonlinear composites incorporating field fluctuations: I—Theory. Journal of the Mechanics and Physics of Solids 50, 737–757.
Ponte Castañeda, P., Tiberio, E., 2000. A second-order homogenization procedure in finite elasticity and applications to black-filled elastomers. Journal of the Mechanics and Physics of Solids 48, 1389–1411.
Quapp, M.K., Weiss, J.A., 1998. Material characterization of human medial collateral ligament. Journal of Biomechanical Engineering 120, 757–763.
Qiu, G.Y., Pence, T.J., 1997. Remarks on the behavior of simple directionally reinforced incompressible nonlinearly elastic solids. Journal of Elasticity 49, 1–30.
Rosen, B.W., 1965. Mechanics of Composite Strengthening. In: Fiber Composite Materials. American Society for Metals 37–75.
Triantafyllidis, N., Abeyaratne, R.C., 1983. Instability of a finitely deformed fiber-reinforced elastic material. Journal of Applied Mechanics 50, 149–156.
Triantafyllidis, N., Maker, B.N., 1985. On the comparison between microscopic and macroscopic instability mechanisms in a class of fiber-reinforced composites. Journal of Applied Mechanics 52, 794–800.
Triantafyllidis, N., Nestorovic, M.D., Schaard, M.W., 2006. Failure surfaces for finitely strained two-phase periodic solids under general in-plane loading. Journal of Applied Mechanics 73, 505–516.
Walpole, L.J., 1969. On the overall elastic moduli of composite materials. Journal of the Mechanics and Physics of Solids 17, 235–251.